Chapter 7

Data Analysis

7.1 Overview

The μSR data in 0.04 μs time bins and six 0.02 wide x bins were fitted to

$$N(t) = N_0[\int C(x)dx + P_\mu A(\tilde{x})G(t)\langle\cos\theta\rangle_t \int D(x)dx]\exp(-t/\tau_\mu) \qquad (7.1)$$

Here C(x) and D(x) are the angle independent and dependent parts respectively of the radiatively corrected (V-A) differential decay rate [section (3.3)] smeared by the e^+ energy-loss straggling (Appendix B) and by a sum of Gaussian momentum resolution functions.

The fit parameters common to all x bins were the μ^+ mean-life τ_μ, the μ^+ spin precession frequency ω and the initial time t_0 incorporated into $\langle\cos\theta\rangle_t$, and the two (one) parameters of the Kubo-Tomita (Gaussian) spin relaxation function G(t) [section (4.4)]. The other fit parameters were the normalizations N_0 and the asymmetries $P_\mu A(\tilde{x})$ relative to the (V-A) prediction for each of the six x bins.

Both the spin-held [Figure (4.1)] and μSR data [Figure (4.3)] are consistent with zero background. Since any fitted positive background would increase the apparent decay asymmetry and thus strengthen the limits on right-handed currents, the μSR data background was fixed to zero. It was checked that the spin-held data exhibited a consistent exponential decay rate over the time range used in the μSR fits.

The maximum likelihood poisson statistics χ^2, defined by

$$\chi^2 = 2\sum_i [e_i - o_i + o_i \ell n(o_i/e_i)]$$

where o_i and e_i are the observed and expected number of events respectively in the i'th bin, was minimized using a double precision version of the MINUIT minimization program.

7.2 Positron Momentum Spectra

Positrons leaving the stopping target and traversing the other material (≈200 mg/cm^2) upstream of the spectrometer are energy-loss straggled to lower momenta where the unstraggled decay asymmetry is less. The e^+ energy-loss straggling therefore increases the apparent asymmetry below the endpoint. Figure (7.1) shows the μSR data momentum spectra for the Al and Al* targets. The greater energy-loss straggling is apparent in the more rounded shoulder in the thicker Al* target data.

The radiatively corrected (V-A) μ^+ differential decay rate [section (3.3)] was evaluated for $\cos\theta=-1,0,1$ at momentum intervals of $\Delta x=0.0004$. These three momentum spectra were energy-loss straggled for both ionization and bremsstrahlung using the formalism of Tsai[49] as described in Appendix B.

The three straggled momentum spectra were then smeared by a sum of three Gaussian momentum resolution functions with standard deviations σ, 2σ, and 3σ determined by fitting the time-average μSR data to a straggled unpolarized ($\cos\theta=0$) momentum spectrum.

The integral of C(x) [equation (7.1)] for each x bin was evaluated by summing the appropriate smeared and straggled decay rate points of the $\cos\theta=0$ spectrum. Similarly the integral of D(x) for each x bin was evaluated by subtracting the sum of the $\cos\theta=-1$ decay rate points from the sum of the $\cos\theta=1$ decay rate points and then dividing by 2.

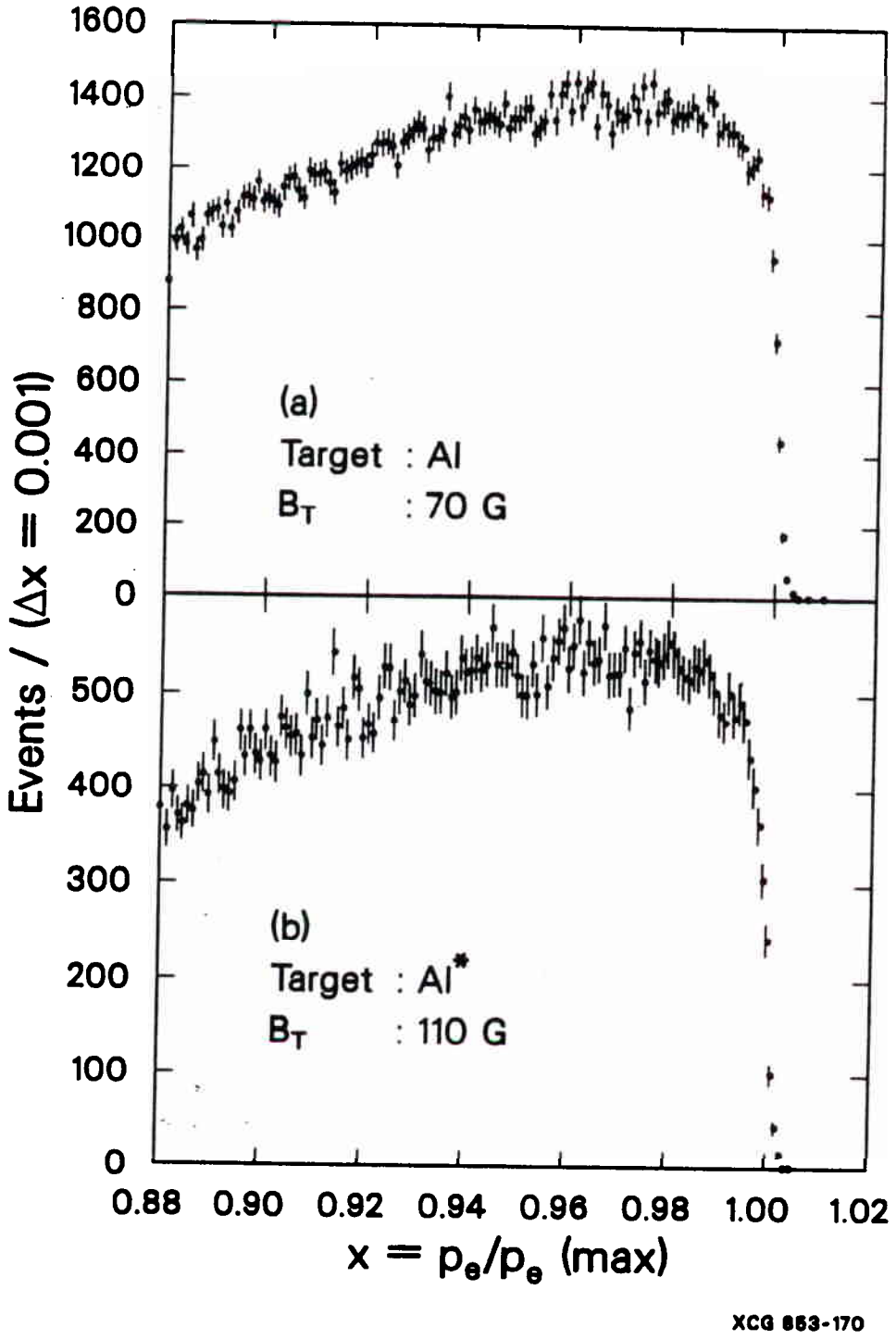

FIGURE (7.1). Momentum spectra of μSR data with (a) Al target and (b) Al* target. Greater energy-loss straggling in the thicker Al* target results in a less sharp edge.

7.3 The Positron Angular Acceptance

The angular acceptance of the apparatus for decay e^+ in each x bin is given by the observed $\hat{p}_e$ distribution observed in time-average isotropic μSR data. In practice one selects a time window which maximizes the number of decay e^+ originating from μ^+ with precessed spin directions averaging to zero polarization. The μ^+ polarization directions $\hat{P}_\mu$, assumed to lie along $-\hat{p}_\mu$ initially, precess with frequency $\omega=g_\mu eB_T/2m_\mu c$. The $\langle\cos\theta\rangle_t$ of equation (7.1) is given at any time t by the mean cosθ between the $\hat{p}_e$ and precessing $\hat{P}_\mu$ distributions. If the distributions contain N events

$$\langle\cos\theta\rangle_t = (1/N^2)\sum_{ij}\sum\cos\theta_{ij}(t) \qquad (7.2)$$

where $\cos\theta_{ij}(t) = (\sin\theta_\mu\cos\phi_\mu)_i(\sin\theta_e\cos\phi_e)_j$

$$+[(\cos\theta_\mu)_i\sin\omega t + (\sin\theta_\mu\sin\phi_\mu)_i\cos\omega t](\sin\theta_e\sin\phi_e)_j$$

$$+[(\cos\theta_\mu)_i\cos\omega t - (\sin\theta_\mu\sin\phi_\mu)_i\sin\omega t](\cos\theta_e)_j$$

Note that if azimuthal symmetry is present equation (7.2) reduces to

$$\langle\cos\theta\rangle_t = \langle\cos\theta_\mu\rangle\langle\cos\theta_e\rangle\cos\omega t \qquad (7.3)$$

Since the precise precession frequency is unknown until the fit is complete, $\langle\cos\theta\rangle_\psi$ is pre-calculated instead for 1° steps of the precession angle $\psi=\omega t$ using equation (7.2). As the fit proceeds variation of the parameters ω and t_o causes the time bins to correspond to different ranges of the 1° precession angle steps. The $\langle\cos\theta\rangle_t$ for a given time bin is then the mean $\langle\cos\theta\rangle_\psi$, weighted for μ^+ decay within the bin, of the precession angle steps or fractions thereof corresponding to that time bin. It should be noted that the time-zero

parameter t_o is well-defined because the observed $\hat{p}_\mu$, and hence $\hat{P}_\mu$, distribution defines the time-zero phase of the μSR signal.

Since the procedure described above is applied to the data in each fit the analysis should be immune to any acceptance changes due, for example, to variations in the μ^+ beam phase space or detector efficiencies provided the reconstructed quantities for any given event are independent of detector efficiency.

7.4 Positron Momentum Acceptance

The e^+ momentum acceptance is a maximum near x=1 and decreases to about 60% of maximum at x=0.88. Approximating the momentum acceptance changes as linear within each of the six x bins allows simple acceptance corrections to be made.

For each x bin the mean x of time-average P_μ=0 μSR data [section (7.3)] is calculated and compared with the corresponding mean x of the theoretical smeared and straggled unpolarized ($\cos\theta$=0) momentum spectrum of section (7.2). If the data mean x lies $\langle\Delta x_d\rangle$ from the bin center while the theoretical mean x is at $\langle\Delta x_t\rangle$, the acceptance correction factor multiplying the theoretical spectra Δx from the bin center is $f(\Delta x) = 1+k\Delta x$ where $k = 3\times10^{4}(\langle\Delta x_d\rangle-\langle\Delta x_t\rangle)$. After applying such corrections to each x bin of the smeared and straggled $\cos\theta$=-1,0,1 momentum spectra the integrals of C(x) and D(x) are calculated as described in section (7.2).

7.5 Monte Carlo Tests

The data fitting method described in the preceding sections was tested using a simple Monte Carlo event generator to produce (V-A) 'events' according to the radiatively corrected decay rate of section (3.3). The fitted asymmetry normalized to that expected for (V-A) decay, $P_\mu A(\tilde{x})$, should be consistent with unity.

Two 'data' sets were generated with different input $\cos\theta_\mu$, $\cos\theta_e$, and momentum acceptance distributions. Each 'data' set contained 2.0×10^6 'events' compared to 0.59×10^6 real events contributing to the final experimental results. The first 'data' set had constant input $\cos\theta_\mu$ (0.99-1.00), $\cos\theta_e$ (0.975-1.000) and x (0.88-1.00) acceptance distributions, and a μ^+ spin precession frequency corresponding to B_T=70-G. For the second 'data' set, generated for B_T=110-G, the input $\cos\theta_\mu$ distribution decreased linearly to zero at $\cos\theta_\mu$=0.99; the $\cos\theta_e$ distribution decreased linearly by 50% from $\cos\theta_e$=1→0.975; and the x acceptance decreased linearly by 40% from x=1→0.88. In both cases the input Gaussian spin relaxation function G(t) reduced the μSR signal amplitude at t=10 μs to 70% of its t=0 value, which was the largest damping observed in the metal target data. No 'events' were generated for t<0.12 μs, again imitating the real data. No apparatus effects were included other than those implicit in the input $\cos\theta_\mu$, $\cos\theta_e$, and x acceptance distributions. The integrals of C(x) and D(x) in equation (7.1) were therefore determined from the momentum spectra of section (3.3) without the energy-loss straggling and smearing described in section (7.2).

The fitted $P_\mu A(\tilde{x})$ averaged over x bins for the two 'data' sets were 0.9996±0.0010 and 0.9998±0.0009. The relative consistency of these

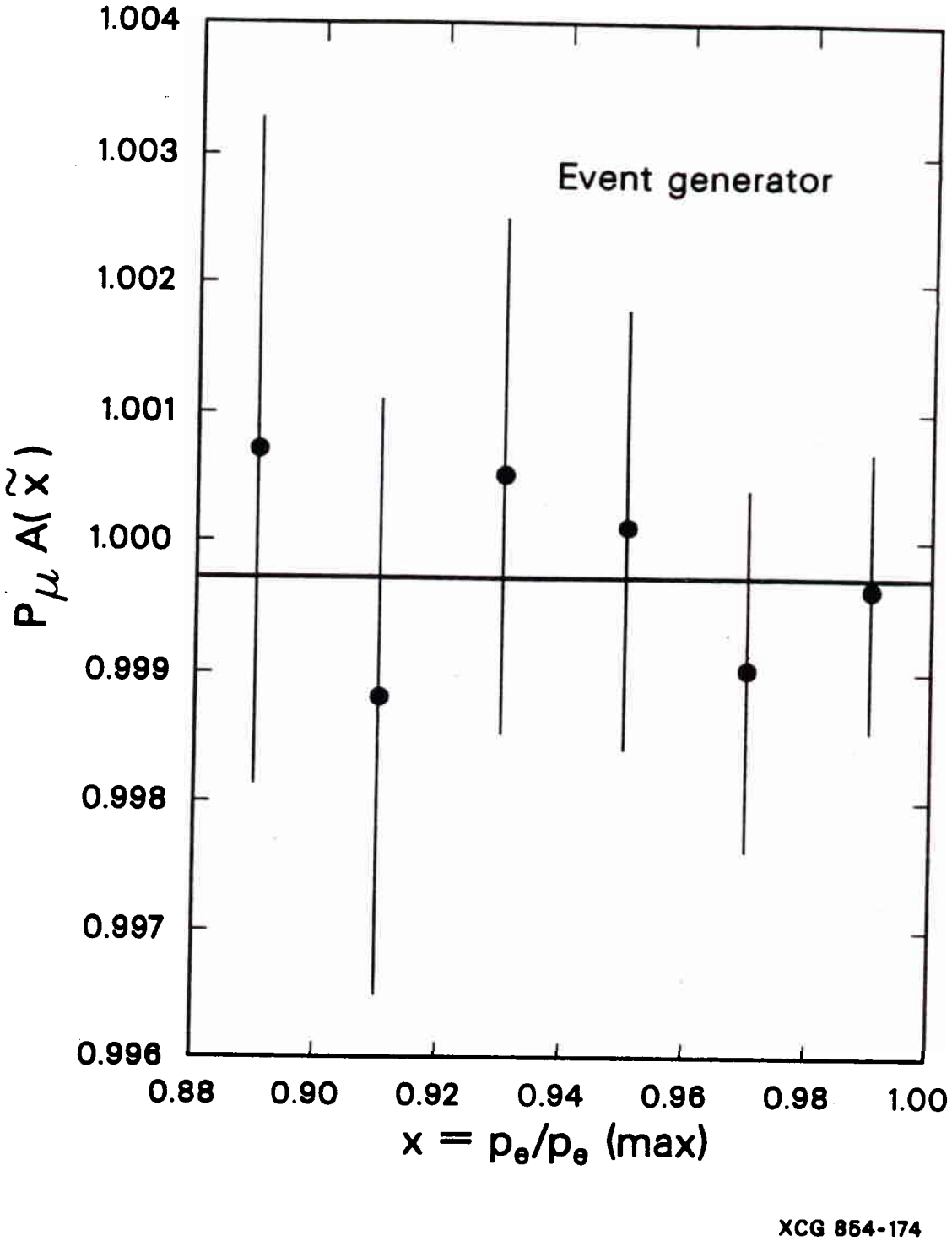

FIGURE (7.2). Fitted $P_\mu A(\tilde{x})$ for 4.0×10^6 Monte Carlo events generated with $P_\mu A(\tilde{x})=1$. The weighted mean fitted $P_\mu A(\tilde{x})=0.9997\pm0.0007$.

values, and of the combined value 0.9997±0.0007 with the input $P_\mu A(\tilde{x})$ of unity at a statistical level 6.7 times that of the real data gives confidence in the fitting procedure. The combined fitted $P_\mu A(\tilde{x})$ for each x bin are plotted in Figure (7.2).

7.6 Data Fitting Results

The results of the various fits described in this section are tabulated in Tables (C.1) and (C.2) of Appendix C. All runs except those with some known deficiency were included in the fits. For example, several runs were rejected because of partial deflation of the helium bag (present only in Run 2) between drift-chambers D2 and D3.

The final results are based on the normalized asymmetries $P_\mu A(\tilde{x})$ fitted to each x bin for the various stopping targets and B_T settings. The results of these fits are shown in Table (C.1) for both Gaussian and Kubo-Tomita μ^+ spin relaxation functions G(t). The fitted initial depolarization (12.4±0.9%) in liquid He may be due to μ^+-e^- spin exchange processes during or shortly after μ^+ thermalization. The fitted $P_\mu A(\tilde{x})$ averaged over x bins for each metal target data set are displayed in Figure (7.3). The Run 2 Cu and Cu* target data exhibits significantly smaller $P_\mu A(\tilde{x})$ [4.8σ for Gaussian G(t)] than the other metal target data. Muon range-straggling calculations [Table (5.2)] show that the 156 mg/cm^2 Cu target was too thin to stop the μ^+ well within the target, while the 222 mg/cm^2 Cu* target, composed of two foils, may have suffered from μ^+ stopping between the foils.

The $P_\mu A(\tilde{x})$ for all x bins and targets should be consistent if the momentum calibration is correct, if the decay parameters ρ and δ have

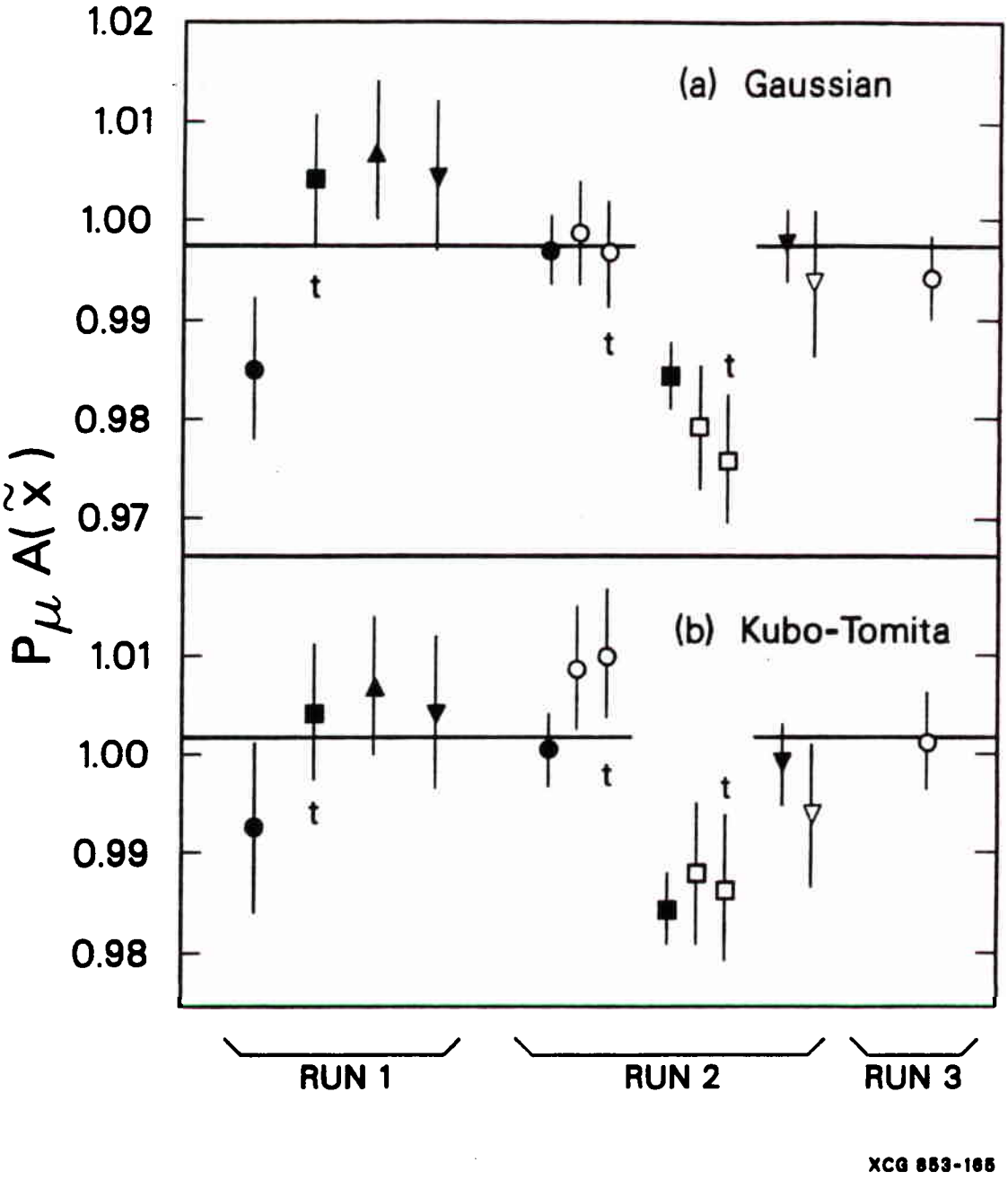

FIGURE (7.3). Weighted mean fitted $P_\mu A(\tilde{x})$ for the metal target data sets with (a) Gaussian and (b) Kubo-Tomita μ^+ spin relaxation forms. Targets are Al (circles), Cu (squares), Ag (triangles) and Au (inverted triangles). Thick targets Al* and Cu* are marked "t". Spin precessing fields are B_T=70-G (closed symbols) and B_T=110-G (open symbols).

their (V±A) values [see equation (3.3)], and if the targets do not produce differing initial μ^+ depolarizations. Excluding the He and Run 2 Cu and Cu* data, the remaining 52 $P_\mu A(\tilde{x})$ values for Gaussian G(t) have a mean of 0.9973±0.0016 with χ^2_{51}=63.5 (C.L.=11%). Inclusion of Run 2 Cu and Cu* yields a mean $P_\mu A(\tilde{x})$ = 0.9934±0.0014 with χ^2_{69}=106.7 (C.L.=0.2%). The final result is based on the metal target data sets excluding Run 2 Cu and Cu*. The Run 1 Cu* data set was retained because there the μ^+ stopped 0.5 rms straggling lengths deeper in the second foil due to the proportional chamber gas being methane/methylal instead of magic gas. The x bin averaged $P_\mu A(\tilde{x})$ in Figure (7.3) for the ten remaining data sets are statistically consistent with χ^2_9=8.4 (C.L.=49%). Figure (7.4) shows the $P_\mu A(\tilde{x})$, averaged over the remaining metal targets, for each x bin with the 1σ possible momentum calibration systematic error added in quadrature to the statistical error. With only the statistical errors the points have χ^2_5=7.5 (C.L.=19%). The line is the best fit using the world average δ and ρ values [section (9.4)].

Table (C.1) shows that for Run 1 Ag, Au, and Cu*, and for Run 2 Au (70-G and 110-G) the Kubo-Tomita G(t) fits did not have χ^2 less than the Gaussian G(t) fits. Since for these data sets the Kubo-Tomita G(t) closely approaches its Gaussian limit the true $P_\mu A(\tilde{x})$ may be less than that obtained with Gaussian G(t). Refitting with a form $G(t)=\exp(-\alpha t^\beta)$ yielded $\beta>2$, lower χ^2, and lower $P_\mu A(\tilde{x})$ for Run 1 Ag, Au, and Cu* but not for Run 2 Au. For the 10 metal targets and Kubo-Tomita G(t) the mean $P_\mu A(\tilde{x})$=1.0020±0.0018. When the lower values for Run 1 Ag, Au, and Cu* are used instead the mean $P_\mu A(\tilde{x})$=1.0013±0.0018, which is still significantly larger than the Gaussian G(t) mean $P_\mu A(\tilde{x})$=0.9973±0.0016. Thus the global use of Gaussian G(t) appears to have provided a lower

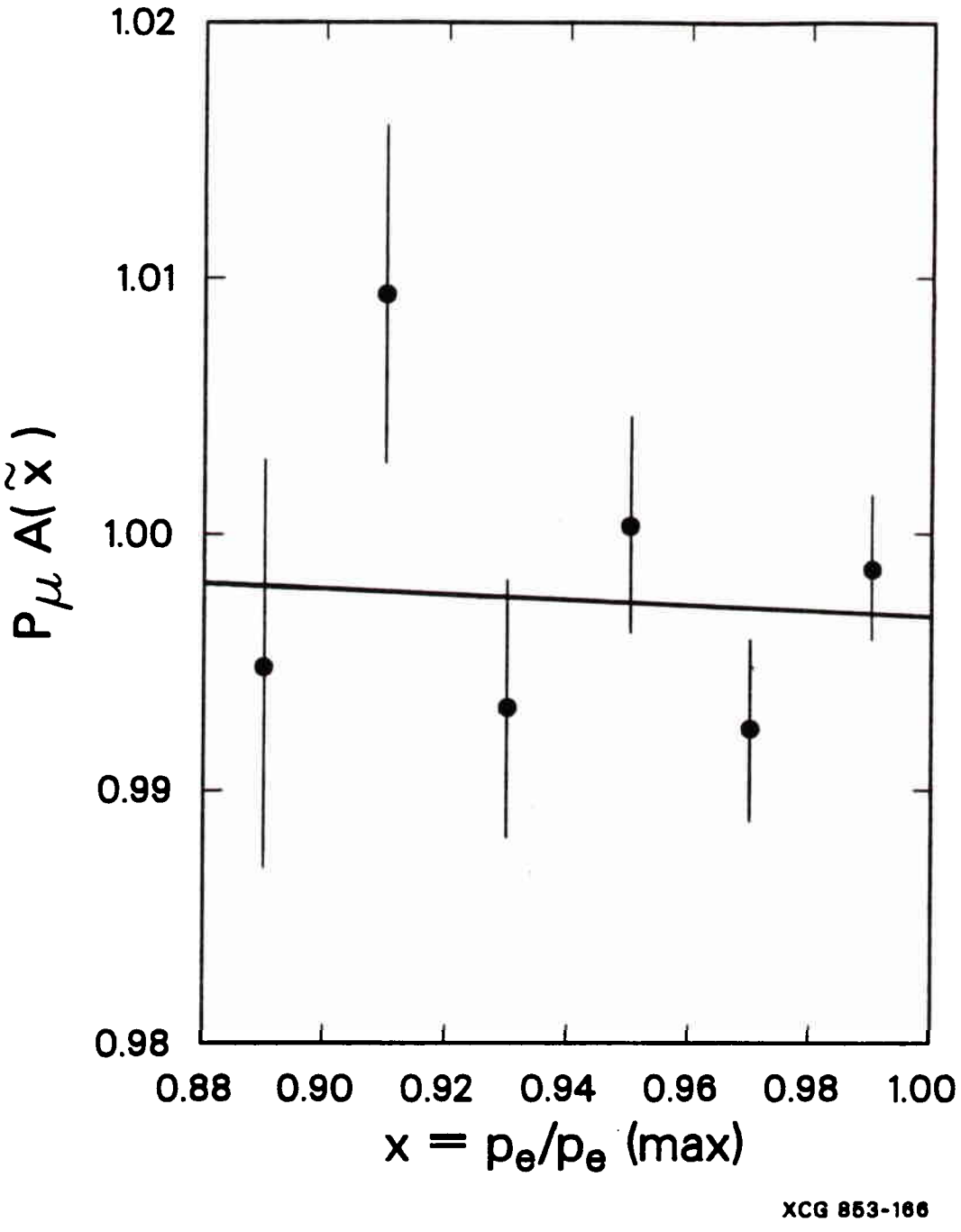

FIGURE (7.4). Weighted mean fitted $P_\mu A(\tilde{x})$ in each x bin for metal targets excluding Run 2 Cu and Cu*. Error bars are statistical errors added in quadrature to the possible momentum calibration systematic error. The fitted line assumes the world average values of δ and ρ.

bound on $P_\mu A(\tilde{x})$.

Three auxiliary fits were made to each data set. Firstly, with G(t) fixed to unity a common $P_\mu A(\tilde{x})G(t)$ was fitted to the x bins for each μ^+ spin precession period. The fitted $P_\mu A(\tilde{x})G(t)$ tabulated in Table (C.1) and plotted in Figure (7.5) versus the time-range midpoint indicate the actual form of G(t). The curves in Figure (7.5) correspond to the Gaussian G(t) obtained in the primary fits. The aluminum target data, which has a significantly better χ^2 for Kubo-Tomita G(t) is seen to exhibit an actual G(t) far closer to Gaussian than exponential. The μSR signal damping in Al is much larger than observed in other experiments, and may be due to μ^+ trapping in cracks or other defects in the cold-rolled Al foils.

Secondly, for each data set a common $P_\mu A(\tilde{x})$ was fitted to the x bins for each of five 0.005 wide $\cos\theta_e$ bins with a Gaussian G(t) fixed to that obtained in the primary fit. The results are shown in Table (C.1). The 50 measurements in the data sets contributing to the final results have χ^2_{44}=52.4 (C.L.=33%). The combined data in Figure (7.6) are consistent (χ^2_4=1.4, C.L.=85%) with fitted $P_\mu A(\tilde{x})$ independent of reconstructed $\cos\theta_e$.

Thirdly, a common $P_\mu A(\tilde{x})$ was fitted to the x bins for individual runs with the Gaussian G(t) obtained in the primary fit for the corresponding data set. The results are tabulated in Table (C.2). Figure (7.7) displays the results as a histogram of the deviation of the individual run $P_\mu A(\tilde{x})$ from the data set mean in units of the individual run statistical error. The histogram is consistent (χ^2_{14}=11.6, C.L.=60%) with a normal distribution truncated at ±4σ. There is no evidence for 'bad' runs apart from those rejected for known

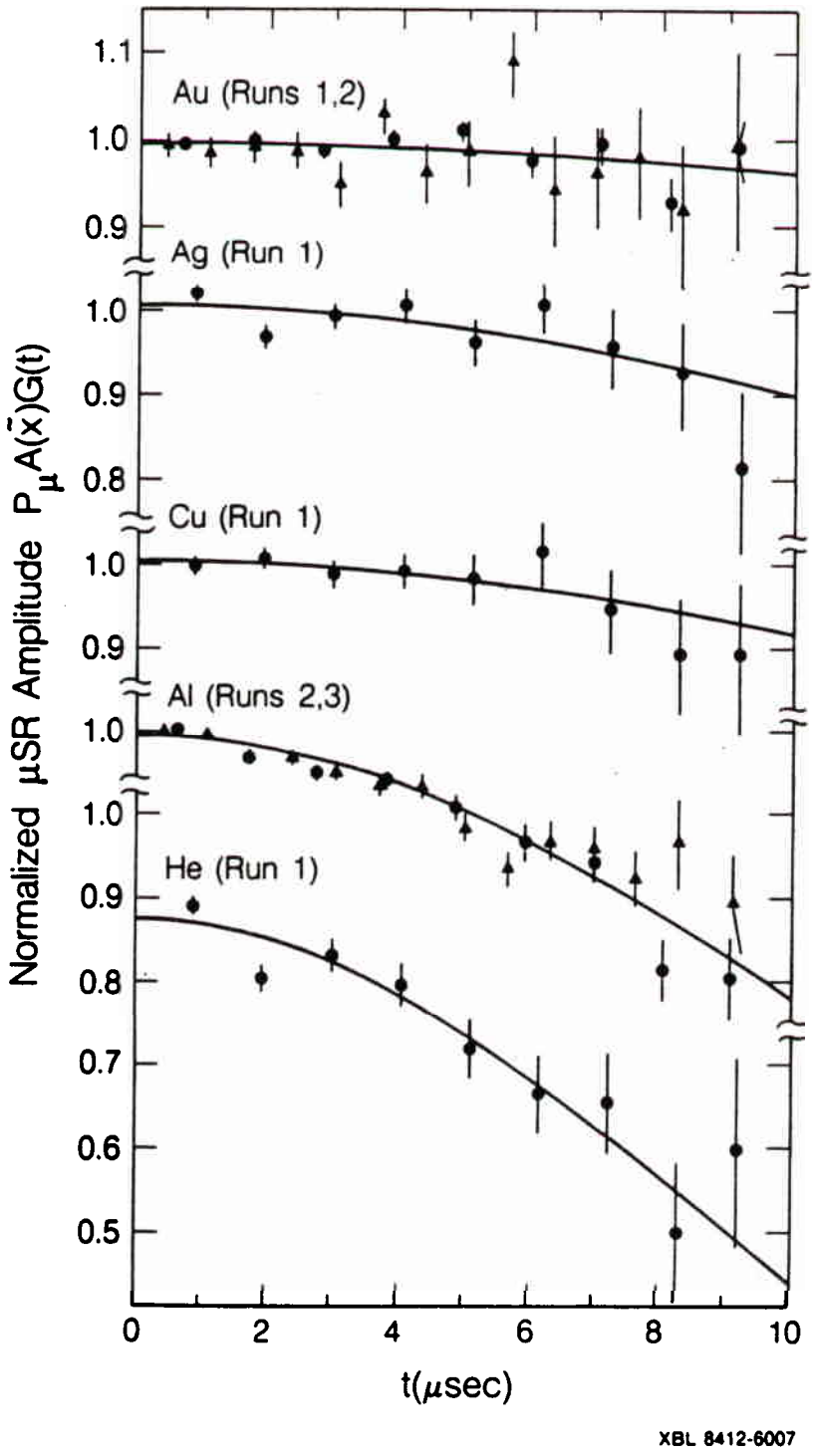

FIGURE (7.5). Values of $P_\mu A(\tilde{x})G(t)$ for each μ^+ spin precession cycle with B_T=70-G (circles) and B_T=110-G (triangles). The curves assume Gaussian μ^+ spin relaxation functions G(t).

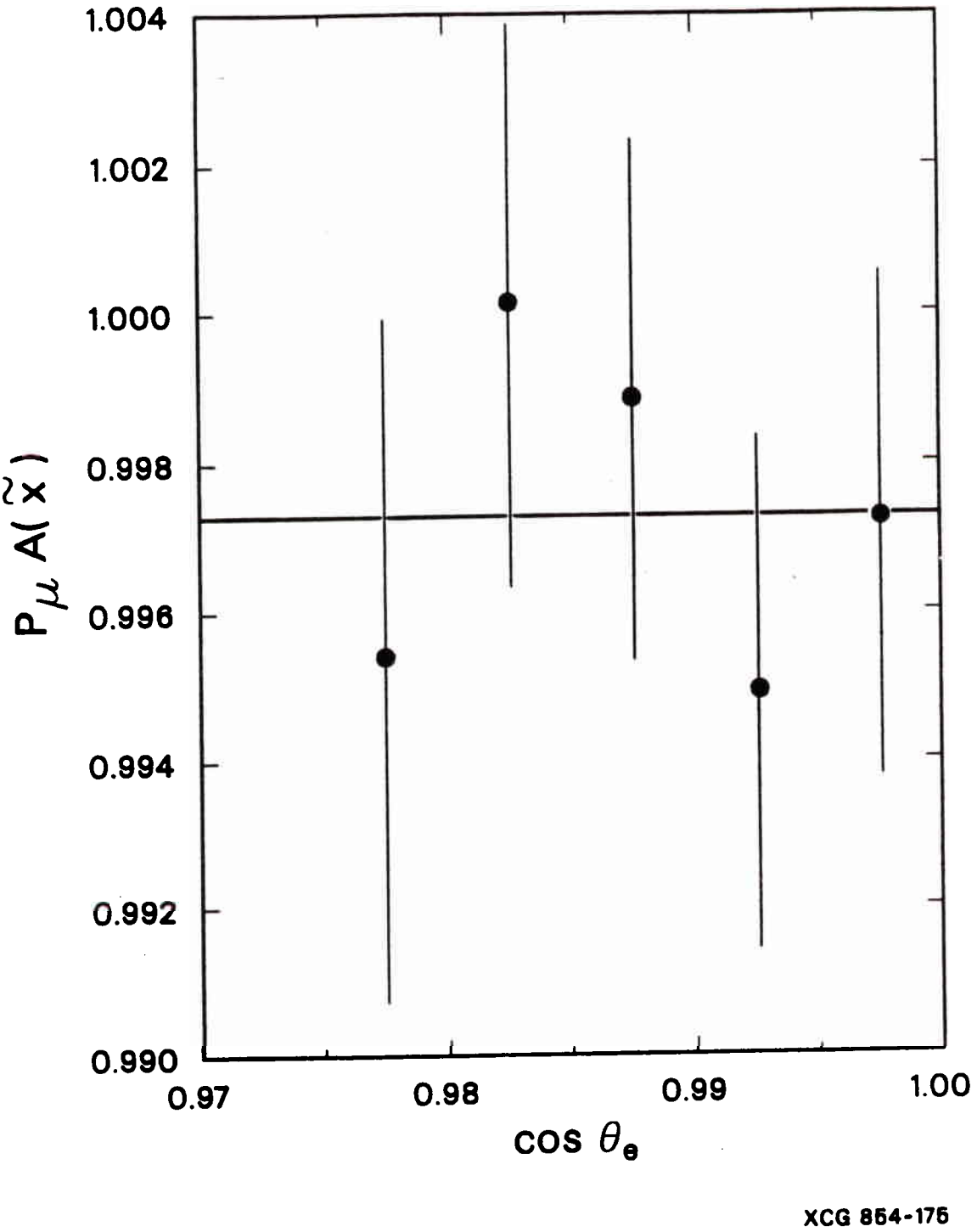

FIGURE (7.6). Weighted mean fitted $P_\mu A(\tilde{x})$ in each $\cos\theta_e$ bin for the metal targets excluding Run 2 Cu and Cu*.

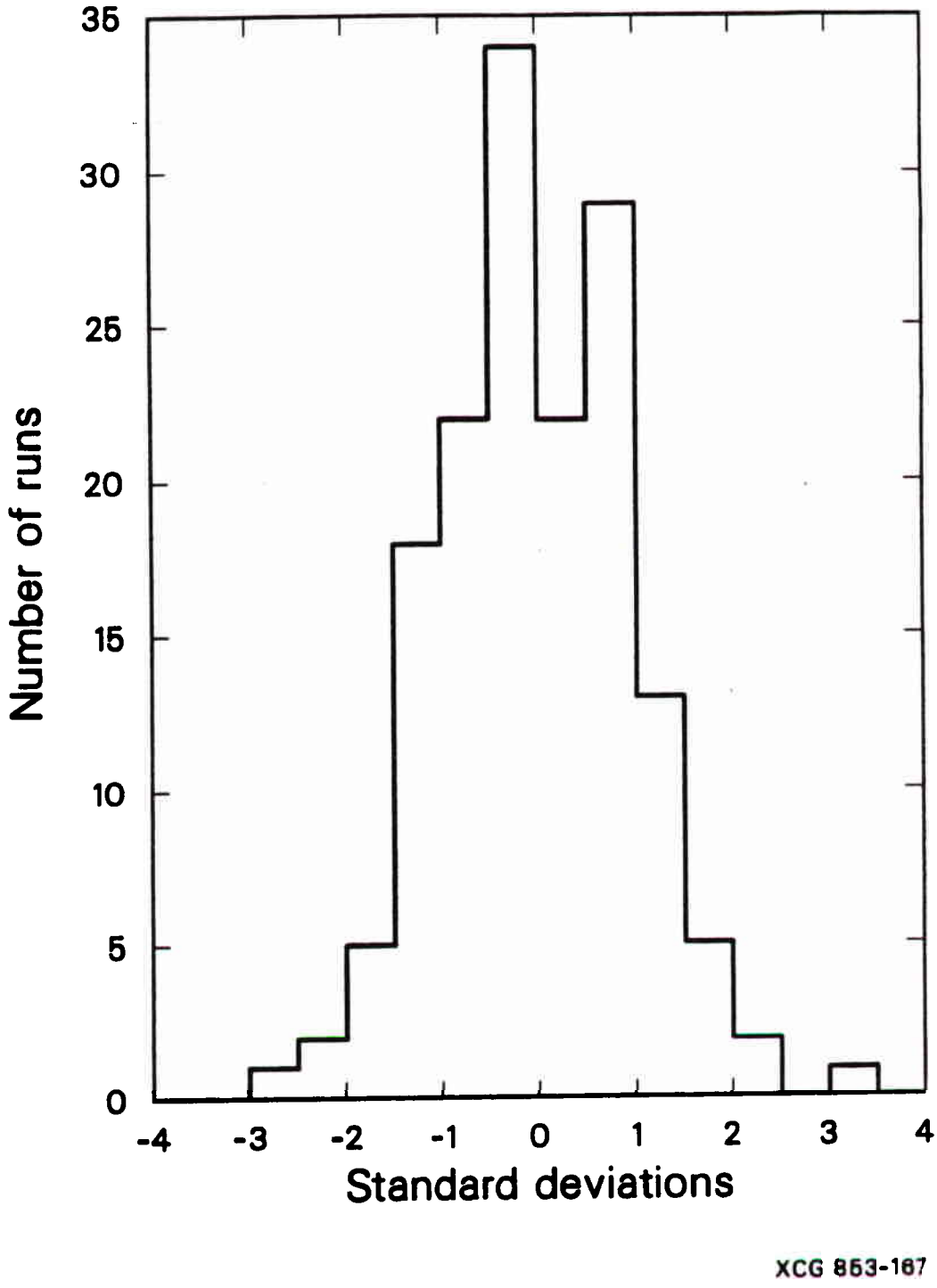

FIGURE (7.7). Histogram of the deviation of the individual run $P_\mu A(\tilde{x})$ from the corresponding data set mean in units of the individual run statistical error. All runs listed in Table (C.2) are included.

deficiencies prior to data fitting. The $P_\mu A(\tilde{x})$ of individual runs contributing to the final results are displayed in the Figure (7.8) histogram.

In each of the three auxiliary fits the μ^+ spin precession frequency, the initial time t_o and the muon mean-life were fixed to the corresponding values determined in the primary fits. The statistical errors on $P_\mu A(\tilde{x})$ in the auxiliary fits have been increased by the 5% required to compensate for the fixed parameters.

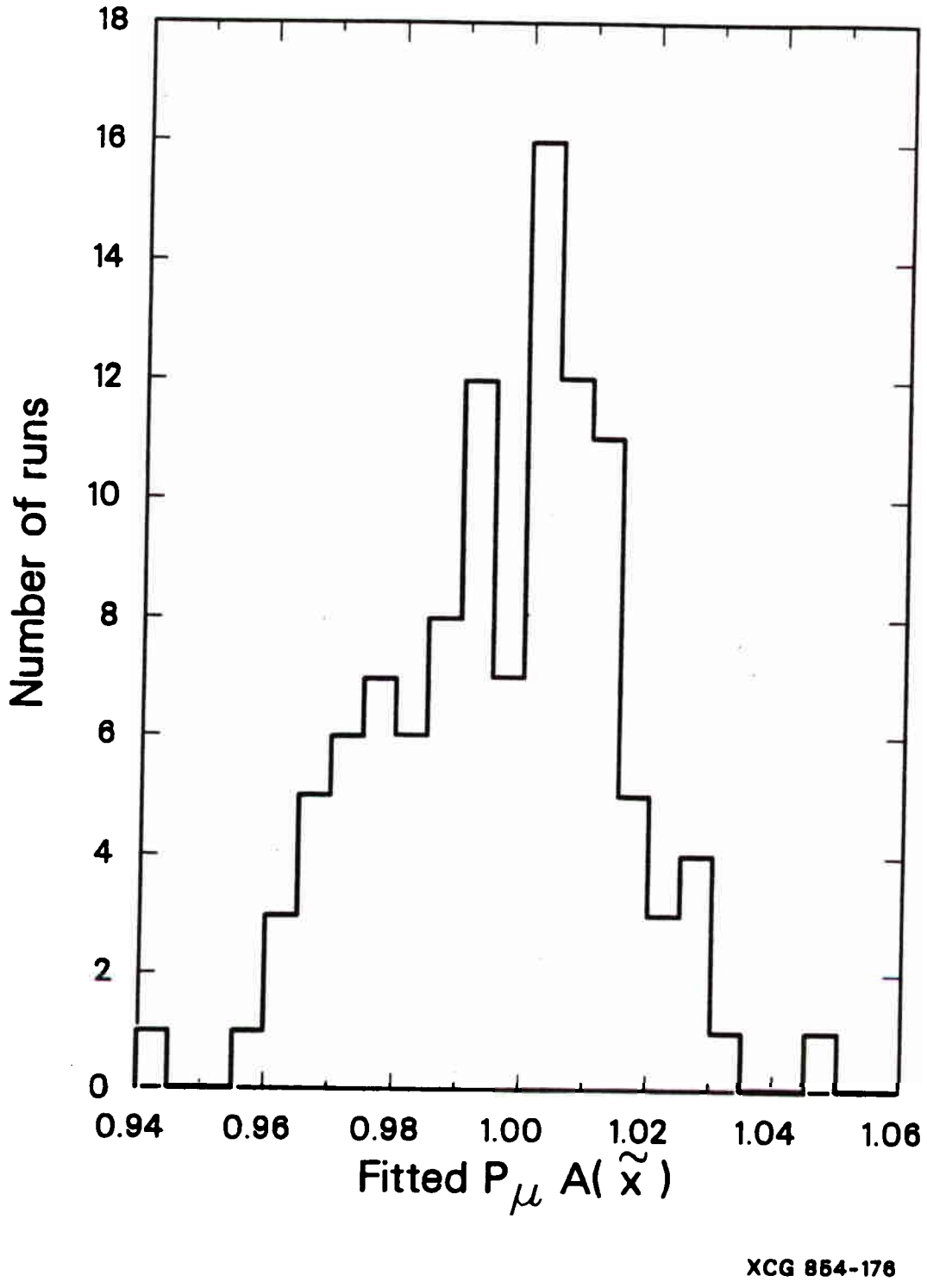

FIGURE (7.8). Histogram of the individual run $P_\mu A(\tilde{x})$ for the metal targets excluding Run 2 Cu and Cu*.

Chapter 8

Corrections and Systematics

8.1 Corrections

8.1.1 Muon Depolarization in Scattering with Electrons

The muon beam polarization is reduced by spin exchange effects in scattering with the unpolarized electrons of the medium[30]. Assuming that the muon energy-loss for E>3 keV is due entirely to scattering with electrons, the calculation in section (4.2) shows the polarization of the stopped beam is 0.9993 of the initial P_μ. A possible error of ±0.0002 is assigned to this estimated depolarization. The fitted values of $P_\mu A(\tilde{x})$ should therefore be corrected upwards by a factor of 1.0007±0.0002.

8.1.2 Coulomb Scattering

The method for obtaining the $\langle\cos\theta\rangle_t$ for each time bin was discussed in section (7.3). It was shown that if azimuthal symmetry applied

$$\langle\cos\theta\rangle_t = \langle\cos\theta_\mu\rangle\langle\cos\theta_e\rangle\cos\omega t$$

Coulomb scattering is relativistically helicity conserving and non-relativistically spin conserving. The non-relativistic limit is assumed to apply to the μ^+, which initially have β=0.27. The effect of multiple Coulomb scattering is to misalign the μ^+ spin and momentum directions, and to misalign the true and measured e^+ emission

directions. Consequently corrections must be made to both $\langle\cos\theta_\mu\rangle$ and $\langle\cos\theta_e\rangle$.

To a good approximation material upstream of the midpoint between proportional chambers P1 and P2, which measure the incoming muon direction, contributes to the misalignment of the μ^+ spin and momentum directions while material downstream of this point does not. However, scattering in the production target material and in the material near P1 require corrections of opposite sign to $\langle\cos\theta_\mu\rangle$. Consider an idealized beamline which admits only μ^+ with momenta along the beam axis after Coulomb scattering in the production target. Suppose the amount of material near P1 is negligibly small. Since the μ^+ spins and momenta are misaligned $|\langle\cos\theta_{\mu,spin}\rangle|<|\langle\cos\theta_\mu\rangle|=1$. Now suppose the amount of production target material is negligibly small so that the μ^+ leave the beamline with spins and momenta aligned along the beam axis. Scattering near P1 leaves the spins aligned along the beam axis and now $|\langle\cos\theta_\mu\rangle|<|\langle\cos\theta_{\mu,spin}\rangle|=1$.

The mean production target thickness traversed by the μ^+ was 6.2 mg/cm^2. The thickness of the other material upstream of the midpoint of P1 and P2 was 18.4 mg/cm^2. Scattering near P1 should therefore dominate, requiring a net upwards correction to $\langle\cos\theta_\mu\rangle$ and a downwards correction to $P_\mu A(\tilde{x})$. It should be noted that acceptance effects and software cuts preferentially reject potential events with the largest μ^+ scattering angles near P1. Detailed Monte Carlo studies using calculations of Molière scattering[50,51] yield a correction for $\langle\cos\theta_\mu\rangle$ of +0.0003, and hence a correction factor for $P_\mu A(\tilde{x})$ of 0.9997. A possible error of ±0.0002 is assigned to the correction.

The e^+ scattering is more transparent. Events in which the e^+ is

scattered out of the angular acceptance, i.e. to $\cos\theta_e<0.975$, are lost while events in which the e^+ are scattered into the angular acceptance are gained. Thus $\langle\cos\theta_{e,true}\rangle < \langle\cos\theta_e\rangle$ and an upwards correction to $P_\mu A(\bar{x})$ is required. Monte Carlo studies yield a correction factor, averaged over the various stopping targets, for $P_\mu A(\bar{x})$ of 1.0002. A possible error of ±0.0001 is assigned to this correction.

8.1.3 Extra Muons

The number N of muons expected to be present in the stopping target is determined by the μ^+ beam rate λ and mean-life τ_μ :

$$\frac{dN}{dt} = \lambda - \frac{N}{\tau_\mu}$$

If the beam is turned on at t=0

$$N(t) = \lambda\tau_\mu[1-\exp(-t/\tau_\mu)]$$

Assuming an average proton current of 80 μA incident on the production target the μ^+ beam rate is estimated to be $\lambda=1.5\times10^4$ Hz from the observed μ-stop rate corrected for dead-time.

Events with extra μ^+ arriving up to 10 μs before the μ-stop are tagged as 'extra-befores' and are rejected. The residual admixture of extra-befores arriving before the 10 μs rejection period is therefore $\lambda\tau_\mu\exp(-10\mu s/\tau_\mu)=3.5\times10^{-4}$. The requirement of continuity between the μ^+ and e^+ tracks at the stopping target [section (6.4)] is estimated to reduce the admixture to 0.9×10^{-4}. Taking these extra-before μ^+ to be time-average unpolarized with respect to the μ-stop muons implies a correction factor of 1.0001 for the fitted $P_\mu A(\bar{x})$. A possible error of

±0.0001 is assigned to this correction.

A similar calculation for extra-after μ^+ arriving unobserved during the 0-0.3 μs notch (Runs 2, 3) in extra-after-1 [section (5.3)] implies correction factors of 1.0005 for B_T=70-G and 1.0011 for B_T=110-G. However, the after-pulsing in P1 and P2 which necessitated the notch cause some extra-after μ^+ arriving within the notch to be observed as after-pulses after the notch. The above corrections are therefore too large. If extra-after-2, with a 0-0.5 μs notch (Runs 2, 3), is used instead of extra-after-1 the mean fitted $P_\mu A(\tilde{x})$ is reduced by 0.0009 whereas the calculated reduction is 0.0013. Thus 30% of the effect appears to be lost to after-pulsing. A larger proportion of extra-after μ^+ arriving within the shorter 0-0.3 μs notch should be observed as after-pulses. It is estimated that the calculated corrections should be reduced by 50%. Averaging over the two B_T values and including the effect of the longer 0.6 μs notch in Run 1 yields a correction factor of 1.0004 for the fitted $P_\mu A(\tilde{x})$. A possible error of ±0.0003 is conservatively assigned to this correction.

8.1.4 Cloud Muons

Figure (5.3) indicates that 98% of cloud μ^+ are eliminated by the rf time cuts. The fitted asymmetry is reduced by 0.015 when no rf time cuts are made. The residual 2% of cloud μ^+ therefore require an estimated correction factor of 1.0003±0.0002 for the fitted $P_\mu A(\tilde{x})$.

8.1.5 Longitudinal Field Component

Any residual longitudinal component in the μ^+ spin precessing field reduces the apparent μSR signal amplitude.

The methods used to null the ≈40-G longitudinal field in the stopping target region [section (5.2.1)] are estimated to leave an rms residual longitudinal field ≈1-G.

In addition the μ^+ experience the longitudinal components of the random local fields due to the nuclear magnetic dipoles. As noted in section (4.4) the local fields are a few Gauss for aluminum and copper. However, at room temperature the μ^+ are mobile and sample many different local fields in succession. The time-average local field seen by the μ^+ is therefore reduced. Assuming a uniform applied transverse field, the local field ΔB is related to the static linewidth σ by equation (4.3): $\langle \Delta B^2 \rangle = 2\sigma^2/\gamma_\mu^2$. Taking σ^2 from fits using the Gaussian spin relaxation function $G(t)=\exp(-\sigma^2 t^2)$ yields effective rms local fields ΔB_{rms} ranging from 0.2-G for the Au target to 1.0-G for the Al target. The rms longitudinal local field component is $\Delta B_{rms}/\sqrt{3}$.

After adding in quadrature to obtain the total longitudinal field B_ℓ, the correction factor for $P_\mu A(\tilde{x})$ is $1/\cos(B_\ell/B_T) = 1.0001$ when averaged over the B_T values. A possible error of ±0.0001 is assigned to this correction.

8.1.6 Timing Errors

Any random spreads in the times attributed to the μ-stop and μ-decay relative to the true times effectively smear the μSR signal, thereby reducing its apparent amplitude. The time spreads of signals

from the left and right photomutlipliers viewing S1 and S2 with respect to the mixed S1 and mixed S2 signals allow an estimate of 2 ns for the rms error on the lifetime of the individual muons. The μ^+ spin precession period is T=1.06 μs for B_T=70-G and T=0.65 μs for B_T=110-G, resulting in a correction factor for $P_\mu A(\tilde{x})$ of $1/\cos(2\pi \times 2ns/T) = 1.0001$ when averaged over B_T values. A possible error of ±0.0001 is assigned to this correction.

8.1.7 Summary

The corrections discussed in the preceding sections are summarized in Table (8.1). The combined correction factor is 1.0016±0.0006. The possible errors in the μ^+ and e^+ Coulomb scattering corrections have been added linearly, as have the possible errors in the extra-before and extra-after muon corrections, before being added in quadrature to the other possible errors.

Source of Correction	Correction Factor
Muon depolarization in scattering with e^-	1.0007 ± 0.0002
Coulomb scattering of muons	0.9997 ± 0.0002
Coulomb scattering of positrons	1.0002 ± 0.0001
Extra-before muons	1.0001 ± 0.0001
Extra-after muons	1.0004 ± 0.0003
Residual cloud muons	1.0003 ± 0.0002
Longitudinal field component	1.0001 ± 0.0001
Timing errors	1.0001 ± 0.0001
Total correction factor	1.0016 ± 0.0006

Table (8.1)

8.2 Systematic Errors

The major sources of possible systematic error, other than those associated with the corrections of section (8.1), are discussed in the following sections. Other possible systematic errors are estimated to be small compared to ±0.0001.

8.2.1 Reconstruction of θ_μ and θ_e

The main sources of possible systematic error in the reconstruction of $\cos\theta_\mu$ and $\cos\theta_e$ are longitudinal misalignment of the wire-chambers and the approximations involved in using the first-order optics formalism (Appendix A) to determine the e^+ track.

A possible error of ±2 mm in the relative longitudinal positions of P1 and P2, and of P3 relative to D1 and D2, correspond to errors of ±0.0002 in $\langle\cos\theta_\mu\rangle$ and $\langle\cos\theta_e\rangle$.

Monte Carlo studies show that the first-order optics formalism reconstructs the e^+ tracks, in the absence of scattering and chamber resolution effects, with an accuracy much better than ±0.0001 in $\langle\cos\theta_e\rangle$. A 10% change in the assumed field strength was shown to cause a change in the reconstructed $\langle\cos\theta_e\rangle$ small compared to 0.0001. In practice minimizing the wire-chamber rms residuals allowed the field scaling factor [95% of the Table (5.1) values] to be determined to ±5%. A more conservative estimate of ±0.0002 for the possible error associated with the first-order optics formalism is adopted here.

The μ^+ and e^+ have radii of curvature of ≈10 m and ≈15 m in the spin precessing field B_T. Ignoring their 5 cm path length through B_T causes a negligible error in the reconstructed $\langle\cos\theta_\mu\rangle$ and $\langle\cos\theta_e\rangle$.

The possible reconstruction errors are therefore estimated to be ± 0.0002 in $\langle \cos\theta_\mu \rangle$ and ± 0.0003 in $\langle \cos\theta_e \rangle$.

8.2.2 Momentum Calibration

The possible errors in the momentum calibration for the various x bins are shown in Table (6.1). Near the (V-A) limit an error Δx in momentum yields

$$\Delta[P_\mu A(\tilde{x})]/P_\mu A(\tilde{x}) = -4\Delta x/(1-4\tilde{x}^2)$$

The momentum calibration contributes a possible error of ± 0.0010 to the determination of the endpoint asymmetry $P_\mu A(0) = \xi P_\mu \delta/\rho$ [section (9.4)].

8.2.3 Definition of x=1

In order to fit the data to the theoretical momemtum spectra it is necessary for their endpoints to coincide. This was achieved by fitting the endpoint positions of both the data and 'events' generated from the theoretical spectra, and adjusting the data x to obtain agreement as discussed in section (6.5). Assigning a possible error of ± 0.0001 to the endpoint agreement yields an error of $\pm 0.04\%$ in the fitted asymmetries, i.e. ± 0.0004 for $P_\mu A(\tilde{x})=1$.

8.2.4 Energy-Loss Straggling

An error of 10% in the amount of downstream material traversed by the e^+ corresponds to an average error of ± 0.0003 in the fitted $P_\mu A(\tilde{x})$.

8.2.5 Muon Mean-Life

The fits described in section (7.6) were performed with the μ^+ mean-life fixed to the mean value obtained for the corresponding run period. The combined mean-life from the three run periods, which used different clocks, is τ_μ=2.209±0.003 μs assuming zero background. The statistical error is ±0.006 μs for free background. A more conservative estimate of ±0.008 μs is adopted here for the possible error in τ_μ. This corresponds to an error of ±0.0003 in the fitted $P_\mu A(\tilde{x})$.

8.2.6 Summary

The possible systematic errors discussed in sections (8.1) and (8.2) are summarized in Table (8.2). The combined possible systematic error is ±0.0013 when averaged over x bins. Table (9.1) shows the possible systematic errors for the individual x bins, which differ due to the momentum calibration contribution.

Source of Possible Error	Error
Muon depolarization in scattering with e^-	±0.0002
Coulomb scattering of muons	±0.0002
Coulomb scattering of positrons	±0.0001
Extra-before muons	±0.0001
Extra-after muons	±0.0003
Cloud muons	±0.0002
Longitudinal field component	±0.0001
Timing errors	±0.0001
Reconstruction of θ_μ	±0.0002
Reconstruction of θ_e	±0.0003
Momentum calibration	±0.0010
Definition of x=1	±0.0004
Positron energy-loss straggling	±0.0003
Muon mean-life τ_μ	±0.0003
Total 1σ possible error	±0.0013

Table (8.2)

Chapter 9

Results and Conclusions

9.1 The Normalized Asymmetries

The weighted mean normalized asymmetries $P_\mu A(\tilde{x})$ of the data sets contributing to the final result are shown in Table (9.1). The corrections discussed in section (8.1) are included and the estimated possible systematic errors discussed in section (8.2) are also shown.

x Range	$P_\mu A(\tilde{x})$	Systematic Error
0.88-0.90	0.9964±0.0074	±0.0029
0.90-0.92	1.0109±0.0062	±0.0024
0.92-0.94	0.9948±0.0047	±0.0018
0.94-0.96	1.0019±0.0040	±0.0015
0.96-0.98	0.9939±0.0034	±0.0011
0.98-1.00	1.0002±0.0028	±0.0009

Table (9.1)

The systematic errors listed in Table (9.1) should be regarded as being completely correlated between the x bins. Thus if the results for N of the x bins are combined the chi-square is given by

$$\chi^2 = \sum_{ij}(p_i-d_i)[V^{-1}]_{ij}(p_j-d_j)$$

where $$V_{ij} = \delta_{ij}\sigma_i^{stat}\sigma_j^{stat} + \sigma_i^{sys}\sigma_j^{sys}$$

and p_i and d_i are the predicted and data values respectively.

9.2 Right-Handed Current Limits With Massless Neutrinos

In left-right symmetric models with massless neutrinos the mass-squared ratio $\varepsilon=M^2(W_1)/M^2(W_2)$ and mixing angle ζ are related to the normalized asymmetries by equation (3.5):

$$P_\mu A(\tilde{x}) = 1 - 2\{2\varepsilon^2 + 2\varepsilon\zeta + \zeta^2[1 + 6\tilde{x}/(1+2\tilde{x})]\}$$

The right-hand side is unchanged if the replacements $\varepsilon\leftrightarrow-\varepsilon$ and $\zeta\leftrightarrow-\zeta$ are made. Fitting the asymmetries in Table (9.1) to equation (3.5) therefore yields two minima of equal chi-square χ_0^2 in the real ε-ζ plane. The physical minimum, denoted by (ε_0,ζ_0), has $\varepsilon_0\geq 0$ whereas $\varepsilon<0$ implies imaginary $M(W_2)$. The 90% confidence limits ($\pm 1.645\sigma_0$) on ζ for $\varepsilon=\varepsilon_0$ correspond to the (ε_0,ζ) for which $\chi^2=\chi_0^2+2.706$. The contour in Figure (9.1) is a curve of constant $\chi^2=\chi_0^2+2.706$ and thus represents a 90% confidence limit in the above sense.

Limits on $M(Z_2)$ are implied by the relation [section (2.2)] $M(Z_2)=M(W_2)\cos\theta_W'/\sqrt{(\cos 2\theta_W')}$. Assuming $M(W_1)=81$ GeV/c^2 and $\sin^2\theta_W'=0.217$ [section (2.1)] the following special case 90% confidence limits are obtained: $M(W_2)>381$ GeV/c^2 and $M(Z_2)>448$ GeV/c^2 for any ζ; $M(W_2)>434$ GeV/c^2 and $M(Z_2)>510$ GeV/c^2 for $\zeta=0$; $|\zeta|<0.044$ for $M(W_2)=\infty$; and $-0.057<\zeta<0.044$ for any $M(W_2)$.

9.3 Limits On $M(W_2)$ With $M(\nu_{\mu R})\neq 0$

The limits obtained in the preceding section assumed massless neutrinos. As discussed in section (2.3) a popular model[15] with Majorana neutrinos has very heavy [$=M(W_2)$] right-handed neutrinos. In that case W_R is decoupled from muon decay and the present experiment

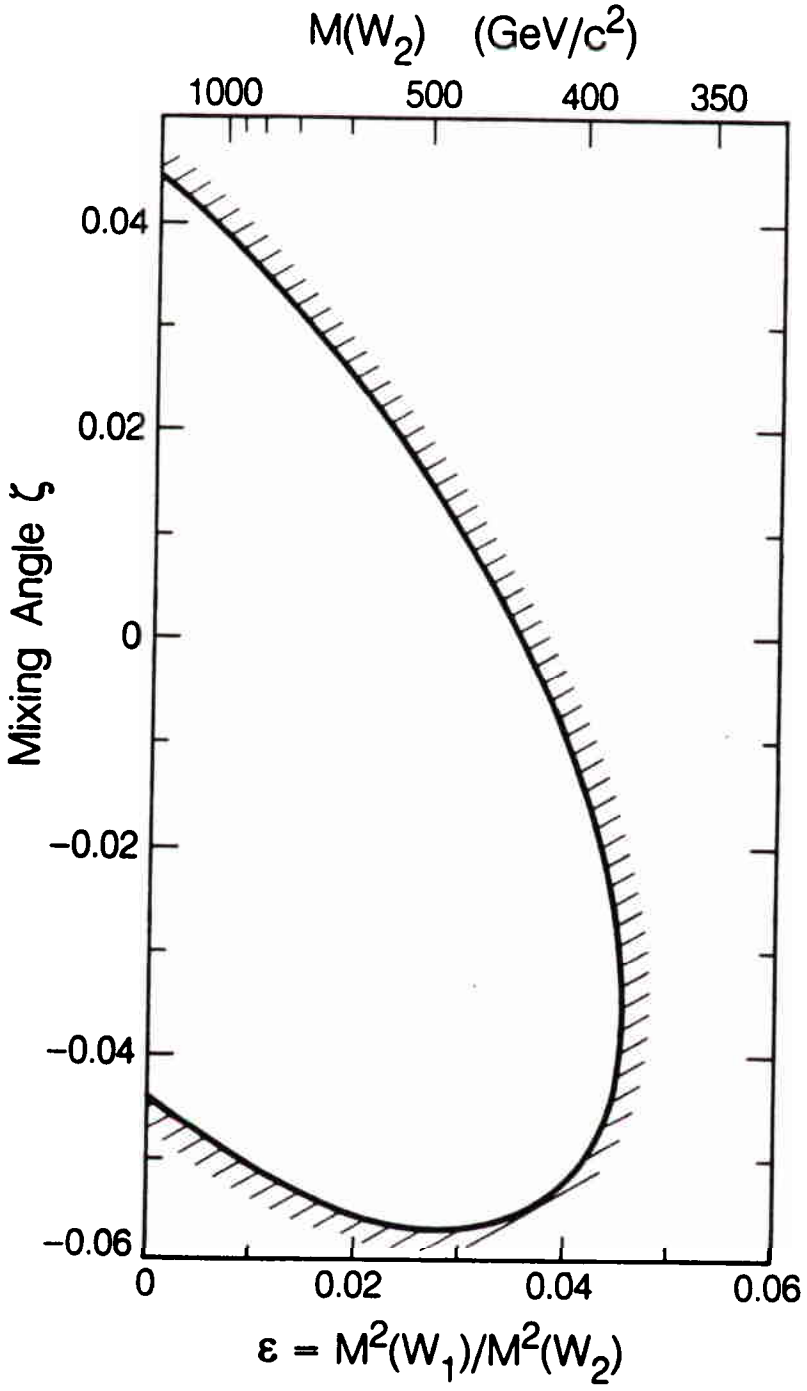

FIGURE (9.1). Contour representing 90% confidence limits on the $W_{1,2}$ mass-squared ratio ε and the left-right mixing angle ζ. The allowed region contains $\varepsilon=\zeta=0$.

sets no limits on right-handed currents. Here limits on $M(W_2)$ are obtained for another possible, if less appealing, scenario: that neutrinos are Majorana particles with $M(\nu_{eR})<<M(\nu_{\mu R})<40$ MeV/c^2 . For simplicity it is assumed that the mixing angle $\zeta=0$ so that $W_2=W_R$.

According to Rekalo[52] the differential decay rate for μ^- via (V-A), and hence for μ^+ via (V+A), including finite ν_μ mass, but neglecting e^- mass and radiative corrections is

$$\frac{d^2\Gamma}{dxd(\cos\theta)} \sim (1-\nu^2/k^2)x^2\{(3-2x)+(3-x)\nu^2/k^2+\cos\theta[1-2x-(1+x)\nu^2/k^2]\} \quad (9.1)$$

where $\nu=M(\nu_\mu)$, $k^2=m_\mu^2-2m_\mu E_e$, and $x=E_e/E_e(max)$ with $E_e(max)=(m_\mu^2-\nu^2)/2m_\mu$.

Limits on $M(W_2)$ as a function of $M(\nu_{\mu R})$ were determined from the normalized asymmetries in Table (9.1). $M(\nu_{\mu R})$=0,14.9,21.1,25.9,29.9, 33.4 and 36.6 MeV/c^2 yield W_R-mediated $E_e(max)$ at the W_L-mediated x=1,0.98,0.96,0.94,0.92,0.90, and 0.88 bin boundaries respectively. Considering only the Table (9.1) asymmetries lying below the W_R-mediated $E_e(max)$ the best fit (V+A) admixture to the (V-A) decay rate was determined for each of the above $M(\nu_{\mu R})$. The μ^+ from W_R-mediated π^+ decay have momenta too low to be accepted by the beamline for all the above $M(\nu_{\mu R})\neq 0$. Since it is assumed here that $\zeta=0$ it follows that the fitted (V+A) admixture is ε^2 for the above $M(\nu_{\mu R})\neq 0$, and $2\varepsilon^2$ for $M(\nu_{\mu R})=0$. The unphysical $\varepsilon^2<0$ region was excluded and 90% confidence lower limits on $M(W_2)$ were determined in the remaining physical region.

The result $M(W_2)>444$ GeV/c^2 for $M(\nu_{\mu R})=0$ is in close but not perfect agreement with the limit $M(W_2)>434$ GeV/c^2 for $\zeta=0$ and $m(\nu)=0$ obtained from the 90% confidence ε-ζ contour in section (9.2).

Accordingly the mass limits found here were reduced by 2% to establish agreement at $m(\nu)=0$. The resulting limits on $M(W_2)$ as a function of $M(\nu_{\mu R})$ are shown in Figure (9.2). The kink near $M(\nu_{\mu R})=5$ MeV/c^2 corresponds to the W_R-mediated π^+ decay μ^+ momentum decreasing below the beam-line setting as $M(\nu_{\mu R})$ increases.

The absence of radiative corrections in equation (9.1) introduces an error into the $M(W_2)$ limits when the (V-A) and (V+A) momentum spectra have different endpoints, i.e. when $M(\nu_{\mu R})\neq 0$. The radiative corrections in section (3.3) reduce the (V-A) decay rate for unpolarized muons by 8.2% at $x=0.99$ and by 3.5% at $x=0.89$. Consequently in the 'worst case' fit, where the $x=0.978$-1.00 W_R-mediated x bin coincides with the $x=0.88$-0.90 W_L-mediated x bin, the fitted ϵ^2 should be ≈5% too small. Increasing the central value of ϵ^2 by 5% for the $M(\nu_{\mu R})=33.4$ MeV/c^2 point reduces the corresponding 90% confidence limit on $M(W_2)$ by only 0.2%. Thus the error introduced by the absence of radiative corrections in equation (9.1) is negligible.

9.4 Limits On $\xi P_\mu \delta/\rho$

The normalized asymmetries $P_\mu A(\tilde{x})$ are related to the muon decay parameters ξ, δ, and ρ by equation (3.3):

$$P_\mu A(\tilde{x}) = (\xi P_\mu \delta/\rho)\{1 + 2\tilde{x}[\tilde{\delta}/(1-2\tilde{x}) - 3\tilde{\rho}/(1+2\tilde{x})]\}$$

The endpoint asymmetry $P_\mu A(0) = \xi P_\mu \delta/\rho$ was obtained by fitting the asymmetries in Table (9.1) by equation (3.3) using the world average value[31] of $\rho=0.7517\pm0.0026$, and $\delta=0.750\pm0.004$ which combines the previous world average value[31] $\delta=0.7551\pm0.0085$ with the preliminary

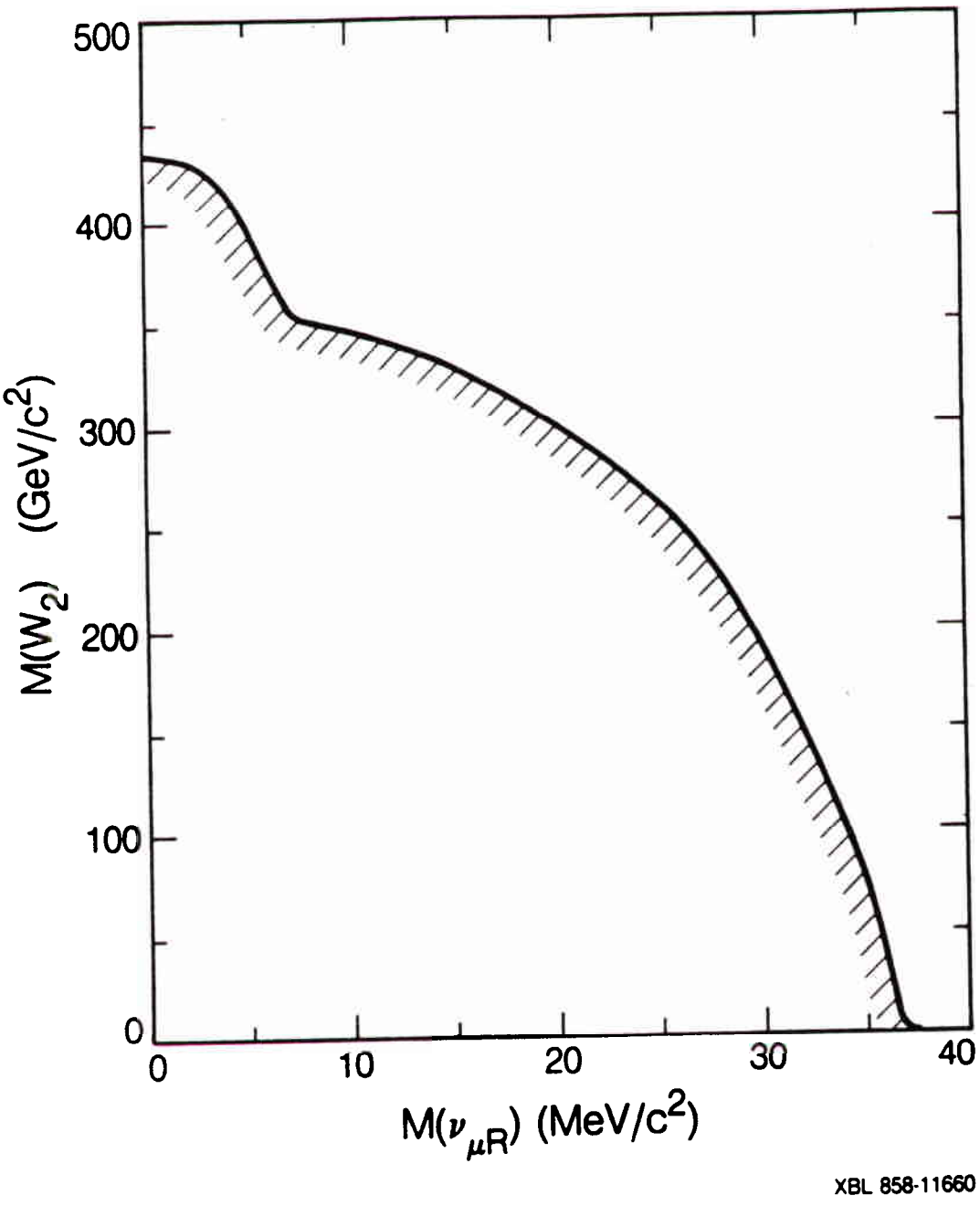

FIGURE (9.2). Contour representing 90% confidence limit on $M(W_2)$ versus the mass of any right-handed ν_μ assuming $M(\nu_{eR}) \ll M(\nu_{\mu R})$. For $M(\nu_{\mu R}) > 5$ MeV/c^2 surface muons from W_R-mediated π^+ decay have momenta below the beamline momentum acceptance. The allowed region lies above the contour.

result[53] $\delta=0.748\pm0.005$ from Run 3 of the present experiment. The fit to the asymmetries before making the correction of +0.0016 discussed in section (8.1) was shown in Figure (7.4). The uncertainties in δ and ρ introduce a possible systematic error of ±0.0009 into the determination of $\xi P_\mu \delta/\rho$. The fitted value is $\xi P_\mu \delta/\rho=0.9984\pm0.0016\pm0.0016$. Since any unknown sources of μ^+ depolarization or any neglected background can only decrease the apparent result, a lower limit for $\xi P_\mu \delta/\rho$ should be quoted. Excluding the unphysical ($\xi P_\mu \delta/\rho>1$) region the 90% confidence limit is $\xi P_\mu \delta/\rho>0.9951$.

9.5 Limits on $M(\nu_{\mu L})$ and $\nu_{\mu L}$ Helicity in π^+ Decay

Limits on the mass of the left-handed muon neutrino and its helicity in pion decay can be deduced from the 90% confidence limit $\xi P_\mu \delta/\rho>0.9951$. The weakest limits are obtained if it is assumed that right-handed currents are absent. In that case $\xi\delta/\rho=1$ and hence $P_\mu>0.9951$. The 90% confidence limit on the $\nu_{\mu L}$ helicity in π^+ decay is then $|h(\nu_{\mu L})|>0.9951$. The corresponding limit on the $\nu_{\mu L}$ velocity $\beta=v/c>0.9951$ in π^+ decay yields the 90% confidence limit $M(\nu_{\mu L})<3.0$ MeV/c^2. For comparison the world average value[31] $M(\nu_{\mu L})<0.5$ MeV/c^2 implies $P_\mu>0.99986$ in the absence of right-handed currents.

9.6 Lorentz Structure Restrictions

The couplings in the helicity projection form of the flavor retention interaction Hamiltonian due to Mursula and Scheck[36] are related to $\xi\delta/\rho$ by equation (3.12). If only one coupling other than the (V-A) coupling $g_{22}=1$ is non-zero the 90% confidence limit $\xi P_\mu \delta/\rho > 0.9951$ restricts $|g_{11}|, |f_{11}| < 0.050$ and $|h_{11}|, |h_{21}| < 0.10$. The relations among the couplings under the assumption of e-μ universality were discussed in section (3.5).

In the special case that the charged current weak interactions are mediated by one heavy spin 1 boson the μ^+ polarization in π^+ decay is given by $P_\mu = (g_{22}-g_{11})/(g_{22}+g_{11})$ and hence $g_{11} < 0.0025$ with 90% confidence.

Mursula and Scheck also considered the case of neutral Q^0 exchange in addition to $W_L^\pm$ exchange. The Q^0 would have total lepton number L=0 but $L_e = \pm 1$ and $L_\mu = \mp 1$. With the new scalar, vector, and tensor couplings denoted by η, γ, and ϕ instead of h, g, and f respectively they find:

$$\xi\delta/\rho \approx 1 - 2(|\gamma_{11}|^2 + |\gamma_{12}|^2 + 4|\phi_{11}|^2)$$

If only one coupling is non-zero the 90% confidence limits are $|\gamma_{11}|, |\gamma_{12}| < 0.050$ and $|\phi_{11}| < 0.025$.

9.7 Limits On Composite Leptons

The possibility that leptons and quarks are composite at some mass scale Λ has received considerable attention in recent years. Among the strongest experimental limits on Λ currently quoted[54,55] are those from Bhabba scattering (>750 GeV), muon (g-2) (>860 GeV), and a more

model-dependent estimate from ν-hadron scattering (>2.5 TeV).

The effects of compositeness may be analyzed in terms of new effective contact interactions. Following the analyses of Peskin[56], and Lane and Barany[57] the most general SU(2)×U(1) invariant contact interaction contributing to $\mu \to e\nu\bar{\nu}$ is

$$\begin{aligned} L_{cont} = (g^2/\Lambda^2)[&\eta_1(\bar{\nu}_{\mu L}\gamma^\kappa\mu_L)(\bar{e}_L\gamma_\kappa\nu_{eL}) + \eta_2(\bar{\nu}_{\mu R}\gamma^\kappa\mu_R)(\bar{e}_R\gamma_\kappa\nu_{eR}) \\ &+ \eta_3(\bar{\nu}_{\mu L}\gamma^\kappa\nu_{eL})(\bar{e}_R\gamma_\kappa\mu_R) + \eta_4(\bar{e}_L\gamma^\kappa\mu_L)(\bar{\nu}_{\mu R}\gamma_\kappa\nu_{eR}) \\ &+ \eta_5(\bar{\nu}_{\mu L}\mu_R)(\bar{e}_L\nu_{eR}) + \eta_6(\bar{\nu}_{\mu L}\nu_{eR})(\bar{e}_L\mu_R) \\ &+ \eta_7(\bar{\nu}_{\mu R}\mu_L)(\bar{e}_R\nu_{eL}) + \eta_8(\bar{\nu}_{\mu R}\nu_{eL})(\bar{e}_R\mu_L) \end{aligned} \tag{9.3}$$

where g is a coupling of hadronic strength; the η_i are of order unity and are normalized so that $|\eta_L|=1$ in the diagonal coupling

$$(g^2/2\Lambda^2)[\eta_L(\bar{e}_L\gamma^\kappa e_L)(\bar{e}_L\gamma_\kappa e_L) + \ldots]$$

The first and second terms in equation (9.3) are purely left-handed and right-handed respectively, and hence are indistinguishable from the usual (V-A) and (V+A) interactions.

There are three special cases of interest:

1. If only left-handed (right-handed) leptons are composite then only the purely left-handed (right-handed) term survives, i.e. only η_1 (η_2) ≠ 0.
2. If both left-handed and right-handed leptons are composite but contain quite different sets of constituents then the purely left-handed and right-handed terms dominate, i.e. $\eta_1, \eta_2 >>$ other η_i.
3. If there is no ν_R, or $M(\nu_R)$ is large, only $\eta_1, \eta_3 \neq 0$.

Assuming an effective interaction Lagrangian $L_{eff} = L_{V-A} + L_{cont}$ yields the endpoint decay rate:

$$1 - P_\mu A(0) = 2(620\text{GeV}/\Lambda)^4 (g^2/4\pi)^2 (\eta_2^2 + \eta_3^2 + \eta_5^2/4)$$

The limit $P_\mu A(0) = \xi P_\mu \delta/\rho > 0.9951$ then implies

$$\Lambda^2 > (2780\text{GeV})^2 (g^2/4\pi) \sqrt{(\eta_2^2 + \eta_3^2 + \eta_5^2/4)}$$

with 90% confidence. (If the not unreasonable assumptions $g^2/4\pi = 2.1$ and $\eta_i > 0.2$ are made, the limit $\Lambda > 2200$ GeV would be obtained.)

For the special cases discussed earlier the limit becomes

1. Only left-handed leptons composite: no limit.

   Only right-handed leptons composite: $\Lambda^2 > (2780\text{GeV})^2 (g^2/4\pi) \eta_2$

2. Left- and right-handed leptons have

   different sets of constituents: $\Lambda^2 > (2780\text{GeV})^2 (g^2/4\pi) \eta_2$

3. No ν_R, or $M(\nu_R)$ large: $\Lambda^2 > (2780\text{GeV})^2 (g^2/4\pi) \eta_3$

Appendix A

First-Order Optics of Solenoidal Fields

This Appendix follows closely a set of notes by K. Halbach[48]. The equation of motion for a particle of momentum $\underset{\sim}{p}$ and charge e in an external magnetic field $\underset{\sim}{B}$ is

$$\dot{\underset{\sim}{p}} = e(\dot{\underset{\sim}{x}} \times \underset{\sim}{B}) \tag{A.1}$$

Evaluation of $\underset{\sim}{\nabla}.\underset{\sim}{B}=0$ on the solenoid axis (z-axis) gives the first order off-axis field components

$$B_x = -xB_z'/2 \quad \text{and} \quad B_y = -yB_z'/2$$

where d/dz is denoted by '.

Then from (A.1)

$$\dot{p}_x = e(\dot{y}B_z + \dot{z}yB_z'/2) \tag{A.2}$$

$$\dot{p}_y = -e(\dot{z}xB_z'/2 + \dot{x}B_z) \tag{A.3}$$

$$\dot{p}_z = e(\dot{y}x - \dot{x}y)B_z'/2 \tag{A.4}$$

With $\dot{z}=v_0$ and $eB_z/mv_0 = B_z/B\rho = k$, where $B\rho$ is the magnetic rigidity of the particle, (A.2) and (A.3) become

$$x'' = y'k + yk'/2$$

$$y'' = -(x'k + xk'/2)$$

which with the notation $w = x+iy$ may be written as

$$w'' = -i(kw' + k'w/2) \tag{A.5}$$

Introducing a new coordinate system $\zeta = \xi+i\eta$ in the w plane, but rotated by $-\alpha$ with respect to $w = x+iy$ gives

$$w = \zeta e^{i\alpha} \tag{A.6}$$

$$w' = (\zeta' + i\alpha'\zeta)e^{i\alpha} \tag{A.7}$$

$$w'' = (\zeta'' + 2i\alpha'\zeta' + i\alpha''\zeta - \alpha'^2\zeta)e^{i\alpha}$$

and from (A.5)

$$\zeta'' + i(2\alpha'+k)\zeta' + (i\alpha''-\alpha'^2-\alpha'k+ik'/2)\zeta = 0$$

Now setting $\alpha' = -k/2$, $\alpha = -(1/2B\rho)\int_0^z B_z(z)dz$ yields

$$\zeta'' + (k/2)^2\zeta = 0 \tag{A.8}$$

The particle motions in the ξ and η directions of the rotating ζ coordinate system are now decoupled:

$$\xi''+(k/2)^2\xi = 0 \quad \text{and} \quad \eta''+(k/2)^2\eta = 0$$

Equation (A.8) has solution

$$\zeta(z) = c_1\cos(kz/2) + c_2\sin(kz/2)$$

and hence $$\zeta'(z) = (k/2)[-c_1\sin(kz/2) + c_2\cos(kz/2)]$$

Choosing the initial conditions $\zeta(0)=\zeta_o$ and $\zeta'(0)=\zeta_o'$ implies $c_1=\zeta_o$ and $c_2=2\zeta_o'/k$. Thus (ζ,ζ') at $z+L$ are related to (ζ_o,ζ_o') at z by

$$\begin{bmatrix}\zeta \\ \zeta'\end{bmatrix} = \begin{bmatrix}\cos(kL/2) & (2/k)\sin(kL/2) \\ -(k/2)\sin(kL/2) & \cos(kL/2)\end{bmatrix}\begin{bmatrix}\zeta_o \\ \zeta_o'\end{bmatrix} \tag{A.9}$$

where $k=\langle B_z \rangle / B\rho$.

The track vector in the laboratory (w) coordinate system is given by (A.6) and (A.7):

$$x+iy = (\xi+i\eta)(\cos\alpha+i\sin\alpha)$$

$$x'+iy' = [\xi'+i\eta'+(\eta-i\xi)k/2](\cos\alpha+i\sin\alpha)$$

Transport matrices between the stopping target and the wire planes of P3-D2 were formed by multiplying together the transport matrices of (A.9) corresponding to successive short steps along the solenoid axis using the field values in Table (5.1). The initial e^+ track vector at the stopping target may then be determined from a least squares fit to the wire chamber space points.

Appendix B

Positron Energy-Loss Straggling

The e^+ lose energy by ionization (including Bhabba scattering) and bremsstrahlung. The ionization energy-loss ΔE has a much shorter tail than the bremsstrahlung, falling as $1/(\Delta E)^2$ versus $1/\Delta E$ for the bremsstrahlung. Comparison of the formulae given by Tsai[4,9] shows that the ionization (bremsstrahlung) process dominates for ΔE less (greater) than about 20-MeV/(Z+2.5) where Z is the atomic number of the material. Since the μSR data x range of 0.88-1.00 corresponds to an energy range of 6.3 MeV both processes must be considered.

According to Tsai[4,9] the probability that an electron with initial energy E_0 has energy $E'>E_0-\Delta_0-\Delta E$ after traversing t radiation lengths, where Δ_0 is the most probable energy-loss due to ionization, is

$$P(E_0,E',t) = (1+0.5772bt)\left[\frac{\Delta E}{E_0}\right]^{bt}\left[1 - \frac{\Gamma}{(1-bt)\Delta E}\right] \qquad (B.1)$$

where $\Gamma = 0.154\text{MeV}(Z/A)g$

with g = number of g/cm^2 for t radiation lengths

and $b = (4/3)[1+(Z+1)/9(Z+\eta)\ln(183Z^{-1/3})]$

with $\eta = \ln(1440Z^{-2/3})/\ln(183Z^{-1/3})$

It follows from equation (B.1) that the probability of the straggled energy lying in the range $E_0-\Delta_0-\Delta E_1 < E'' < E_0-\Delta_0-\Delta E_2$ is

$$P(E_0,E'',t) = \frac{1+0.5772bt}{E_0{}^{bt}}\{[\Delta E_1{}^{bt}-\Delta E_2{}^{bt}] - \frac{\Gamma}{1-bt}[\Delta E_1{}^{bt-1}-\Delta E_2{}^{bt-1}]\} \qquad (B.2)$$

The radiatively corrected (V-A) differential decay rate [section

(3.3)] was evaluated for $\cos\theta=-1,0,1$ at momentum intervals of $\Delta x=0.0004$ in the range $x=0.88-1.00$. These three momentum spectra were straggled according to equation (B.2) ignoring the most probable ionization energy-loss Δ_0 which is essentially constant over the x range of interest. Equation (B.2) is valid for $\Delta E \geq 10\Gamma$. Consequently the stopping target material and the other material upstream of the spectrometer traversed by the e^+ were each divided into 10 steps and the straggling was performed by successive application of equation (B.2).

Appendix C

Tables of Data Fit Results

Run Period : 1
Target : Ag
B_T : 70-G
Events Fitted: 24457

x Range	$P_\mu A(\tilde{x})$ Gaussian	$P_\mu A(\tilde{x})$ Kubo-Tomita
0.92-0.94	$0.9796^{+0.0194}_{-0.0197}$	$0.9798^{+0.0194}_{-0.0198}$
0.94-0.96	$1.0144^{+0.0160}_{-0.0164}$	$1.0145^{+0.0161}_{-0.0165}$
0.96-0.98	$1.0125^{+0.0132}_{-0.0136}$	$1.0127^{+0.0132}_{-0.0137}$
0.98-1.00	$1.0085^{+0.0105}_{-0.0111}$	$1.0087^{+0.0105}_{-0.0112}$
Mean $P_\mu A(\tilde{x})$	$1.0068^{+0.0070}_{-0.0071}$	$1.0070^{+0.0070}_{-0.0071}$
	χ^2_{913}= 887.35	χ^2_{912}= 887.36

$\cos\theta_e$ Range	$P_\mu A(\tilde{x})$ (Gaussian)
0.975-0.980	$0.9978^{+0.0172}_{-0.0181}$
0.980-0.985	$0.9921^{+0.0159}_{-0.0166}$
0.985-0.990	$1.0272^{+0.0141}_{-0.0150}$
0.990-0.995	$1.0004^{+0.0143}_{-0.0151}$
0.995-1.000	$1.0156^{+0.0138}_{-0.0150}$

t(μs)	$P_\mu A(\tilde{x})G(t)$
0.89	$1.0211^{+0.0095}_{-0.0101}$
1.94	$0.9679^{+0.0145}_{-0.0150}$
3.00	$0.9941^{+0.0156}_{-0.0168}$
4.06	$1.0073^{+0.0193}_{-0.0214}$
5.11	$0.9632^{+0.0273}_{-0.0294}$
6.17	$1.0083^{+0.0272}_{-0.0342}$
7.22	$0.9582^{+0.0445}_{-0.0511}$
8.28	$0.9270^{+0.0587}_{-0.0684}$
9.20	$0.8137^{+0.0905}_{-0.1005}$

Table (C.1)...

Run Period : 1
Target : Al
B_T : 70-G
Events Fitted: 27410

x Range	$P_\mu A(\tilde{x})$ Gaussian	$P_\mu A(\tilde{x})$ Kubo-Tomita
0.92-0.94	$0.9928^{+0.0191}_{-0.0194}$	$0.9980^{+0.0211}_{-0.0205}$
0.94-0.96	$1.0006^{+0.0156}_{-0.0160}$	$1.0055^{+0.0182}_{-0.0172}$
0.96-0.98	$0.9842^{+0.0131}_{-0.0135}$	$0.9896^{+0.0173}_{-0.0151}$
0.98-1.00	$0.9743^{+0.0116}_{-0.0121}$	$0.9798^{+0.0168}_{-0.0138}$
Mean $P_\mu A(\tilde{x})$	$0.9849^{+0.0071}_{-0.0072}$	$0.9927^{+0.0089}_{-0.0087}$
	χ^2_{913}= 916.57	χ^2_{912}= 915.73

$\cos\theta_e$ Range	$P_\mu A(\tilde{x})$ (Gaussian)
0.975-0.980	$1.0024^{+0.0156}_{-0.0165}$
0.980-0.985	$1.0081^{+0.0140}_{-0.0148}$
0.985-0.990	$0.9701^{+0.0143}_{-0.0149}$
0.990-0.995	$0.9728^{+0.0150}_{-0.0156}$
0.995-1.000	$0.9699^{+0.0169}_{-0.0176}$

t(μs)	$P_\mu A(\tilde{x})G(t)$
0.89	$0.9867^{+0.0101}_{-0.0105}$
1.94	$0.9817^{+0.0128}_{-0.0134}$
3.00	$0.9585^{+0.0167}_{-0.0175}$
4.06	$0.9792^{+0.0194}_{-0.0209}$
5.11	$0.9184^{+0.0276}_{-0.0295}$
6.17	$0.9012^{+0.0388}_{-0.0416}$
7.22	$0.9325^{+0.0490}_{-0.0533}$
8.28	$0.9135^{+0.0561}_{-0.0624}$
9.20	$0.9754^{+0.0605}_{-0.0775}$

Table (C.1) cont.

Run Period : 1
Target : Au
B_T : 70-G
Events Fitted: 20174

x Range	$P_\mu A(\tilde{x})$ Gaussian	$P_\mu A(\tilde{x})$ Kubo-Tomita
0.92-0.94	$1.0051^{+0.0209}_{-0.0213}$	$1.0051^{+0.0209}_{-0.0214}$
0.94-0.96	$1.0357^{+0.0174}_{-0.0179}$	$1.0357^{+0.0175}_{-0.0180}$
0.96-0.98	$0.9957^{+0.0146}_{-0.0151}$	$0.9957^{+0.0146}_{-0.0151}$
0.98-1.00	$0.9951^{+0.0120}_{-0.0128}$	$0.9951^{+0.0120}_{-0.0128}$
Mean $P_\mu A(\tilde{x})$	$1.0040^{+0.0077}_{-0.0077}$	$1.0040^{+0.0077}_{-0.0077}$
	χ^2_{913}= 1015.16	χ^2_{912}= 1015.18

$\cos\theta_e$ Range	$P_\mu A(\tilde{x})$ (Gaussian)
0.975-0.980	$1.0223^{+0.0164}_{-0.0177}$
0.980-0.985	$0.9931^{+0.0165}_{-0.0174}$
0.985-0.990	$1.0046^{+0.0160}_{-0.0170}$
0.990-0.995	$1.0179^{+0.0167}_{-0.0176}$
0.995-1.000	$0.9839^{+0.0170}_{-0.0184}$

t (μs)	$P_\mu A(\tilde{x})G(t)$
0.89	$0.9815^{+0.0119}_{-0.0124}$
1.94	$1.0205^{+0.0122}_{-0.0135}$
3.00	$0.9797^{+0.0176}_{-0.0189}$
4.06	$1.0216^{+0.0218}_{-0.0238}$
5.11	$1.0357^{+0.0150}_{-0.0227}$
6.17	$0.9078^{+0.0431}_{-0.0464}$
7.22	$0.9075^{+0.0548}_{-0.0614}$
8.28	$0.9456^{+0.0723}_{-0.0800}$
9.20	$0.6744^{+0.1176}_{-0.1286}$

Table (C.1) cont.

Run Period : 1
Target : Cu*
B_T : 70-G
Events Fitted: 23734

x Range	$P_\mu A(\tilde{x})$ Gaussian	$P_\mu A(\tilde{x})$ Kubo-Tomita
0.92-0.94	$0.9930^{+0.0195}_{-0.0199}$	$0.9930^{-0.0195}_{-0.0199}$
0.94-0.96	$0.9904^{+0.0167}_{-0.0171}$	$0.9905^{+0.0167}_{-0.0171}$
0.96-0.98	$1.0004^{+0.0138}_{-0.0142}$	$1.0005^{+0.0138}_{-0.0143}$
0.98-1.00	$1.0145^{+0.0097}_{-0.0104}$	$1.0145^{+0.0097}_{-0.0104}$
Mean $P_\mu A(\tilde{x})$	$1.0040^{+0.0069}_{-0.0070}$	$1.0041^{+0.0069}_{-0.0070}$
	$\chi^2_{913} = 936.60$	$\chi^2_{912} = 936.60$

$\cos\theta_e$ Range	$P_\mu A(\tilde{x})$ (Gaussian)
0.975-0.980	$0.9916^{+0.0171}_{-0.0181}$
0.980-0.985	$1.0091^{+0.0155}_{-0.0164}$
0.985-0.990	$0.9968^{+0.0151}_{-0.0160}$
0.990-0.995	$0.9957^{+0.0144}_{-0.0154}$
0.995-1.000	$1.0341^{+0.0139}_{-0.0155}$

t (μs)	$P_\mu A(\tilde{x})G(t)$
0.89	$0.9988^{+0.0109}_{-0.0114}$
1.94	$1.0078^{+0.0126}_{-0.0135}$
3.00	$0.9890^{+0.0156}_{-0.0169}$
4.06	$0.9929^{+0.0201}_{-0.0218}$
5.11	$0.9841^{+0.0287}_{-0.0314}$
6.17	$1.0156^{+0.0359}_{-0.0395}$
7.22	$0.9471^{+0.0471}_{-0.0538}$
8.28	$0.8947^{+0.0644}_{-0.0717}$
9.20	$0.8932^{+0.0852}_{-0.0983}$

Table (C.1) cont.

Run Period : 1
Target : He
B_T : 70-G
Events Fitted: 28547

x Range	$P_\mu A(\tilde{x})$ Gaussian	$P_\mu A(\tilde{x})$ Kubo-Tomita
0.92-0.94	$0.8645^{+0.0209}_{-0.0212}$	$0.9124^{+0.0246}_{-0.0247}$
0.94-0.96	$0.8835^{+0.0183}_{-0.0184}$	$0.9321^{+0.0220}_{-0.0222}$
0.96-0.98	$0.8906^{+0.0160}_{-0.0162}$	$0.9396^{+0.0198}_{-0.0199}$
0.98-1.00	$0.8653^{+0.0153}_{-0.0156}$	$0.9147^{+0.0191}_{-0.0194}$
Mean $P_\mu A(\tilde{x})$	$0.8764^{+0.0087}_{-0.0087}$	$0.9252^{+0.0106}_{-0.0106}$
	χ^2_{913} = 910.98	χ^2_{912} = 906.92

$\cos\theta_e$ Range	$P_\mu A(\tilde{x})$ (Gaussian)
0.975-0.980	$0.8956^{+0.0196}_{-0.0202}$
0.980-0.985	$0.8715^{+0.0190}_{-0.0194}$
0.985-0.990	$0.8511^{+0.0186}_{-0.0189}$
0.990-0.995	$0.8900^{+0.0183}_{-0.0187}$
0.995-1.000	$0.8791^{+0.0201}_{-0.0206}$

t (μs)	$P_\mu A(\tilde{x})G(t)$
0.89	$0.8912^{+0.0115}_{-0.0118}$
1.94	$0.8042^{+0.0161}_{-0.0164}$
3.00	$0.8322^{+0.0202}_{-0.0207}$
4.06	$0.7975^{+0.0259}_{-0.0267}$
5.11	$0.7208^{+0.0359}_{-0.0370}$
6.17	$0.6660^{+0.0467}_{-0.0482}$
7.22	$0.6550^{+0.0589}_{-0.0614}$
8.28	$0.4992^{+0.0827}_{-0.0851}$
9.20	$0.5976^{+0.1107}_{-0.1168}$

Table (C.1) cont.

Run Period : 2
Target : Al
B_T : 70-G
Events Fitted: 143335

x Range	$P_\mu A(\tilde{x})$ Gaussian	$P_\mu A(\tilde{x})$ Kubo-Tomita
0.88-0.90	$1.0061^{+0.0139}_{-0.0140}$	$1.0089^{+0.0141}_{-0.0143}$
0.90-0.92	$1.0171^{+0.0118}_{-0.0119}$	$1.0200^{+0.0121}_{-0.0123}$
0.92-0.94	$0.9679^{+0.0103}_{-0.0103}$	$0.9707^{+0.0104}_{-0.0105}$
0.94-0.96	$0.9995^{+0.0086}_{-0.0087}$	$1.0025^{+0.0089}_{-0.0092}$
0.96-0.98	$0.9922^{+0.0074}_{-0.0075}$	$0.9952^{+0.0088}_{-0.0076}$
0.98-1.00	$1.0032^{+0.0062}_{-0.0064}$	$1.0064^{+0.0081}_{-0.0064}$
Mean $P_\mu A(\tilde{x})$	$0.9971^{+0.0036}_{-0.0036}$	$1.0004^{+0.0038}_{-0.0038}$
	$\chi^2_{1443} = 1529.28$	$\chi^2_{1442} = 1528.77$

$\cos\theta_e$ Range	$P_\mu A(\tilde{x})$ (Gaussian)
0.975-0.980	$0.9844^{+0.0109}_{-0.0112}$
0.980-0.985	$0.9925^{+0.0082}_{-0.0083}$
0.985-0.990	$1.0081^{+0.0074}_{-0.0076}$
0.990-0.995	$0.9992^{+0.0072}_{-0.0073}$
0.995-1.000	$0.9936^{+0.0071}_{-0.0072}$

t (μs)	$P_\mu A(\tilde{x})G(t)$
0.64	$1.0027^{+0.0051}_{-0.0052}$
1.70	$0.9685^{+0.0068}_{-0.0069}$
2.76	$0.9508^{+0.0088}_{-0.0090}$
3.82	$0.9427^{+0.0109}_{-0.0112}$
4.87	$0.9107^{+0.0146}_{-0.0149}$
5.93	$0.8707^{+0.0205}_{-0.0210}$
6.99	$0.8484^{+0.0251}_{-0.0260}$
8.05	$0.7220^{+0.0349}_{-0.0358}$
9.08	$0.7112^{+0.0477}_{-0.0492}$

Table (C.1) cont.

Run Period : 2
Target : Au
B_T : 70-G
Events Fitted: 111158

x Range	$P_\mu A(\tilde{x})$ Gaussian	$P_\mu A(\tilde{x})$ Kubo-Tomita
0.88-0.90	$1.0188^{+0.0150}_{-0.0152}$	$1.0195^{+0.0153}_{-0.0155}$
0.90-0.92	$1.0250^{+0.0124}_{-0.0125}$	$1.0257^{+0.0129}_{-0.0129}$
0.92-0.94	$0.9839^{+0.0108}_{-0.0109}$	$0.9846^{+0.0113}_{-0.0113}$
0.94-0.96	$0.9976^{+0.0092}_{-0.0093}$	$0.9983^{+0.0100}_{-0.0098}$
0.96-0.98	$0.9924^{+0.0078}_{-0.0080}$	$0.9931^{+0.0095}_{-0.0085}$
0.98-1.00	$0.9949^{+0.0063}_{-0.0066}$	$0.9957^{+0.0080}_{-0.0072}$
Mean $P_\mu A(\tilde{x})$	$0.9975^{+0.0037}_{-0.0037}$	$0.9989^{+0.0043}_{-0.0042}$
	$\chi^2_{1443} = 1510.97$	$\chi^2_{1442} = 1510.99$

$\cos\theta_e$ Range	$P_\mu A(\tilde{x})$ (Gaussian)
0.975-0.980	$0.9905^{+0.0114}_{-0.0117}$
0.980-0.985	$1.0129^{+0.0085}_{-0.0087}$
0.985-0.990	$0.9911^{+0.0080}_{-0.0082}$
0.990-0.995	$0.9922^{+0.0075}_{-0.0077}$
0.995-1.000	$0.9989^{+0.0074}_{-0.0076}$

t (μs)	$P_\mu A(\tilde{x})G(t)$
0.64	$0.9989^{+0.0057}_{-0.0058}$
1.70	$0.9944^{+0.0072}_{-0.0074}$
2.76	$0.9916^{+0.0089}_{-0.0092}$
3.82	$0.9981^{+0.0115}_{-0.0120}$
4.87	$0.9978^{+0.0138}_{-0.0147}$
5.93	$0.9888^{+0.0182}_{-0.0194}$
6.99	$1.0065^{+0.0213}_{-0.0240}$
8.05	$0.9231^{+0.0344}_{-0.0365}$
9.08	$1.0166^{+0.0343}_{-0.0395}$

Table (C.1) cont.

Run Period : 2
Target : Cu
B_T : 70-G
Events Fitted: 129820

x Range	$P_\mu A(\tilde{x})$ Gaussian	$P_\mu A(\tilde{x})$ Kubo-Tomita
0.88-0.90	$0.9977^{+0.0143}_{-0.0144}$	$0.9977^{+0.0142}_{-0.0144}$
0.90-0.92	$0.9838^{+0.0120}_{-0.0121}$	$0.9839^{+0.0119}_{-0.0121}$
0.92-0.94	$0.9928^{+0.0101}_{-0.0102}$	$0.9929^{+0.0101}_{-0.0102}$
0.94-0.96	$0.9819^{+0.0088}_{-0.0089}$	$0.9820^{+0.0088}_{-0.0089}$
0.96-0.98	$0.9851^{+0.0075}_{-0.0076}$	$0.9852^{+0.0075}_{-0.0076}$
0.98-1.00	$0.9796^{+0.0064}_{-0.0065}$	$0.9797^{+0.0064}_{-0.0065}$
Mean $P_\mu A(\tilde{x})$	$0.9844^{+0.0036}_{-0.0036}$	$0.9845^{+0.0036}_{-0.0036}$
	$\chi^2_{1443} = 1424.57$	$\chi^2_{1442} = 1424.54$

$\cos\theta_e$ Range	$P_\mu A(\tilde{x})$ (Gaussian)
0.975-0.980	$0.9865^{+0.0088}_{-0.0090}$
0.980-0.985	$0.9823^{+0.0082}_{-0.0084}$
0.985-0.990	$0.9915^{+0.0077}_{-0.0079}$
0.990-0.995	$0.9806^{+0.0075}_{-0.0076}$
0.995-1.000	$0.9866^{+0.0071}_{-0.0072}$

t (μs)	$P_\mu A(\tilde{x})G(t)$
0.64	$0.9841^{+0.0054}_{-0.0054}$
1.70	$0.9792^{+0.0071}_{-0.0072}$
2.76	$0.9792^{+0.0086}_{-0.0088}$
3.82	$0.9641^{+0.0114}_{-0.0117}$
4.87	$0.9799^{+0.0135}_{-0.0140}$
5.93	$0.9340^{+0.0192}_{-0.0200}$
6.99	$0.9289^{+0.0247}_{-0.0259}$
8.05	$0.9656^{+0.0283}_{-0.0304}$
9.08	$0.9123^{+0.0444}_{-0.0476}$

Table (C.1) cont.

Run Period 2; Target = Al; B_T = 110-G; Events Fitted = 58529

x Range	$P_\mu A(\tilde{x})$ Gaussian	$P_\mu A(\tilde{x})$ Kubo-Tomita
0.88-0.90	$0.9839^{+0.0212}_{-0.0214}$	$0.9940^{+0.0227}_{-0.0225}$
0.90-0.92	$1.0187^{+0.0178}_{-0.0180}$	$1.0290^{+0.0195}_{-0.0193}$
0.92-0.94	$1.0163^{+0.0154}_{-0.0157}$	$1.0260^{+0.0171}_{-0.0169}$
0.94-0.96	$1.0026^{+0.0130}_{-0.0133}$	$1.0117^{+0.0149}_{-0.0146}$
0.96-0.98	$0.9946^{+0.0110}_{-0.0113}$	$1.0033^{+0.0130}_{-0.0126}$
0.98-1.00	$0.9909^{+0.0096}_{-0.0100}$	$1.0000^{+0.0119}_{-0.0115}$
Mean $P_\mu A(\tilde{x})$	$0.9988^{+0.0054}_{-0.0054}$	$1.0090^{+0.0062}_{-0.0062}$
	χ^2_{1443}= 1525.59	χ^2_{1442}= 1522.12

$\cos\theta_e$ Range	$P_\mu A(\tilde{x})$ (Gaussian)
0.975-0.980	$0.9864^{+0.0170}_{-0.0176}$
0.980-0.985	$0.9844^{+0.0130}_{-0.0133}$
0.985-0.990	$1.0084^{+0.0114}_{-0.0118}$
0.990-0.995	$0.9956^{+0.0110}_{-0.0114}$
0.995-1.000	$1.0092^{+0.0105}_{-0.0109}$

t (μs)	$P_\mu A(\tilde{x})G(t)$
0.44	$0.9991^{+0.0092}_{-0.0095}$
1.09	$1.0004^{+0.0101}_{-0.0106}$
1.75	$0.9765^{+0.0130}_{-0.0135}$
2.40	$0.9729^{+0.0151}_{-0.0157}$
3.05	$0.9375^{+0.0191}_{-0.0198}$
3.71	$0.9461^{+0.0212}_{-0.0223}$
4.36	$0.9333^{+0.0252}_{-0.0265}$
5.01	$0.8778^{+0.0302}_{-0.0316}$
5.67	$0.7990^{+0.0388}_{-0.0404}$
6.32	$0.8596^{+0.0418}_{-0.0443}$
6.97	$0.8437^{+0.0488}_{-0.0520}$
7.63	$0.8129^{+0.0571}_{-0.0613}$
8.28	$0.8483^{+0.0619}_{-0.0751}$
9.10	$0.7861^{+0.0742}_{-0.0798}$

Table (C.1) cont.

Run Period 2; Target = Al*; B_T = 110-G; Events Fitted = 55445

x Range	$P_\mu A(\tilde{x})$ Gaussian	$P_\mu A(\tilde{x})$ Kubo-Tomita
0.88-0.90	$0.9701^{+0.0221}_{-0.0224}$	$0.9832^{+0.0230}_{-0.0245}$
0.90-0.92	$0.9857^{+0.0185}_{-0.0187}$	$0.9989^{+0.0222}_{-0.0193}$
0.92-0.94	$1.0046^{+0.0156}_{-0.0158}$	$1.0191^{+0.0243}_{-0.0166}$
0.94-0.96	$0.9929^{+0.0134}_{-0.0136}$	$1.0067^{+0.0208}_{-0.0166}$
0.96-0.98	$1.0034^{+0.0109}_{-0.0112}$	$1.0167^{+0.0120}_{-0.0143}$
0.98-1.00	$0.9991^{+0.0090}_{-0.0095}$	$1.0117^{+0.0181}_{-0.0103}$
Mean $P_\mu A(\tilde{x})$	$0.9968^{+0.0054}_{-0.0055}$	$1.0100^{+0.0067}_{-0.0064}$
	χ^2_{1443}= 1537.18	χ^2_{1442}= 1533.17

$\cos\theta_e$ Range	$P_\mu A(\tilde{x})$ (Gaussian)
0.975-0.980	$1.0116^{+0.0151}_{-0.0158}$
0.980-0.985	$0.9864^{+0.0122}_{-0.0127}$
0.985-0.990	$1.0070^{+0.0113}_{-0.0117}$
0.990-0.995	$0.9933^{+0.0112}_{-0.0115}$
0.995-1.000	$0.9938^{+0.0106}_{-0.0107}$

t (μs)	$P_\mu A(\tilde{x})G(t)$
0.44	$1.0011^{+0.0090}_{-0.0094}$
1.09	$1.0097^{+0.0104}_{-0.0110}$
1.75	$0.9606^{+0.0136}_{-0.0141}$
2.40	$0.9798^{+0.0153}_{-0.0160}$
3.05	$0.9592^{+0.0196}_{-0.0204}$
3.71	$0.9042^{+0.0239}_{-0.0247}$
4.36	$0.9359^{+0.0259}_{-0.0273}$
5.01	$0.8902^{+0.0324}_{-0.0338}$
5.67	$0.9028^{+0.0353}_{-0.0376}$
6.32	$0.9033^{+0.0419}_{-0.0449}$
6.97	$0.8621^{+0.0501}_{-0.0534}$
7.63	$0.7901^{+0.0632}_{-0.0669}$
8.28	$0.8946^{+0.0712}_{-0.0781}$
9.10	$0.8177^{+0.0829}_{-0.0895}$

Table (C.1) cont.

Run Period 2; Target = Au; B_T = 110-G; Events Fitted = 28456

x Range	$P_\mu A(\tilde{x})$ Gaussian	$P_\mu A(\tilde{x})$ Kubo-Tomita
0.88-0.90	$0.9756^{+0.0290}_{-0.0295}$	$0.9756^{+0.0290}_{-0.0295}$
0.90-0.92	$1.0264^{+0.0243}_{-0.0247}$	$1.0264^{+0.0243}_{-0.0247}$
0.92-0.94	$0.9886^{+0.0210}_{-0.0215}$	$0.9886^{+0.0211}_{-0.0214}$
0.94-0.96	$1.0144^{+0.0174}_{-0.0179}$	$1.0144^{+0.0174}_{-0.0179}$
0.96-0.98	$0.9698^{+0.0154}_{-0.0159}$	$0.9697^{+0.0155}_{-0.0159}$
0.98-1.00	$0.9969^{+0.0122}_{-0.0131}$	$0.9969^{+0.0123}_{-0.0131}$
Mean $P_\mu A(\tilde{x})$	$0.9939^{+0.0074}_{-0.0074}$	$0.9939^{+0.0074}_{-0.0074}$
	χ^2_{1443}= 1561.77	χ^2_{1442}= 1561.77

$\cos\theta_e$ Range	$P_\mu A(\tilde{x})$ (Gaussian)
0.975-0.980	$0.9664^{+0.0253}_{-0.0263}$
0.980-0.985	$1.0041^{+0.0159}_{-0.0169}$
0.985-0.990	$0.9774^{+0.0153}_{-0.0160}$
0.990-0.995	$1.0215^{+0.0136}_{-0.0146}$
0.995-1.000	$0.9854^{+0.0150}_{-0.0158}$

t (μs)	$P_\mu A(\tilde{x})G(t)$
0.44	$0.9955^{+0.0129}_{-0.0137}$
1.09	$0.9874^{+0.0169}_{-0.0175}$
1.75	$0.9936^{+0.0174}_{-0.0184}$
2.40	$0.9902^{+0.0203}_{-0.0217}$
3.05	$0.9517^{+0.0262}_{-0.0277}$
3.71	$1.0311^{+0.0167}_{-0.0228}$
4.36	$0.9655^{+0.0321}_{-0.0355}$
5.01	$0.9875^{+0.0354}_{-0.0409}$
5.67	$1.0901^{+0.0354}_{-0.0424}$
6.32	$0.9435^{+0.0611}_{-0.0667}$
6.97	$0.9614^{+0.0525}_{-0.0630}$
7.63	$0.9824^{+0.0561}_{-0.0713}$
8.28	$0.9185^{+0.0762}_{-0.0948}$
9.10	$0.9928^{+0.1075}_{-0.1224}$

Table (C.1) cont.

Run Period 2; Target = Cu; B_T = 110-G; Events Fitted = 41924

x Range	$P_\mu A(\tilde{x})$ Gaussian	$P_\mu A(\tilde{x})$ Kubo-Tomita
0.88-0.90	$0.9758^{+0.0245}_{-0.0248}$	$0.9838^{+0.0256}_{-0.0257}$
0.90-0.92	$0.9701^{+0.0211}_{-0.0214}$	$0.9779^{+0.0223}_{-0.0224}$
0.92-0.94	$0.9900^{+0.0180}_{-0.0183}$	$0.9982^{+0.0194}_{-0.0195}$
0.94-0.96	$1.0216^{+0.0143}_{-0.0146}$	$1.0298^{+0.0159}_{-0.0161}$
0.96-0.98	$0.9783^{+0.0129}_{-0.0132}$	$0.9866^{+0.0146}_{-0.0147}$
0.98-1.00	$0.9514^{+0.0120}_{-0.0124}$	$0.9594^{+0.0138}_{-0.0140}$
Mean $P_\mu A(\tilde{x})$	$0.9795^{+0.0064}_{-0.0064}$	$0.9882^{+0.0071}_{-0.0071}$
	χ^2_{1443}= 1478.43	χ^2_{1442}= 1477.57

$\cos\theta_e$ Range	$P_\mu A(\tilde{x})$ (Gaussian)
0.975-0.980	$0.9699^{+0.0156}_{-0.0162}$
0.980-0.985	$0.9590^{+0.0142}_{-0.0146}$
0.985-0.990	$0.9819^{+0.0131}_{-0.0136}$
0.990-0.995	$0.9758^{+0.0131}_{-0.0135}$
0.995-1.000	$0.9932^{+0.0117}_{-0.0122}$

t (μs)	$P_\mu A(\tilde{x})G(t)$
0.44	$0.9812^{+0.0114}_{-0.0117}$
1.09	$0.9991^{+0.0127}_{-0.0133}$
1.75	$0.9556^{+0.0157}_{-0.0164}$
2.40	$0.9530^{+0.0185}_{-0.0192}$
3.05	$0.9698^{+0.0198}_{-0.0210}$
3.71	$0.9393^{+0.0241}_{-0.0255}$
4.36	$0.9452^{+0.0277}_{-0.0298}$
5.01	$0.9481^{+0.0337}_{-0.0361}$
5.67	$0.9846^{+0.0301}_{-0.0346}$
6.32	$0.9768^{+0.0457}_{-0.0498}$
6.97	$0.9663^{+0.0470}_{-0.0551}$
7.63	$0.9420^{+0.0588}_{-0.0658}$
8.28	$0.9413^{+0.0614}_{-0.0732}$
9.10	$0.8869^{+0.0776}_{-0.0898}$

Table (C.1) cont.

Run Period 2; Target = Cu*; B_T = 110-G; Events Fitted = 39244

x Range	$P_\mu A(\tilde{x})$ Gaussian	$P_\mu A(\tilde{x})$ Kubo-Tomita
0.88-0.90	$0.9577^{+0.0258}_{-0.0262}$	$0.9680^{+0.0269}_{-0.0273}$
0.90-0.92	$0.9682^{+0.0216}_{-0.0220}$	$0.9795^{+0.0230}_{-0.0233}$
0.92-0.94	$0.9641^{+0.0189}_{-0.0192}$	$0.9747^{+0.0205}_{-0.0205}$
0.94-0.96	$0.9704^{+0.0159}_{-0.0162}$	$0.9813^{+0.0172}_{-0.0178}$
0.96-0.98	$0.9938^{+0.0129}_{-0.0133}$	$1.0053^{+0.0150}_{-0.0153}$
0.98-1.00	$0.9759^{+0.0114}_{-0.0119}$	$0.9873^{+0.0133}_{-0.0139}$
Mean $P_\mu A(\tilde{x})$	$0.9760^{+0.0065}_{-0.0066}$	$0.9865^{+0.0073}_{-0.0074}$
	χ^2_{1443}= 1521.30	χ^2_{1442}= 1519.18

$\cos\theta_e$ Range	$P_\mu A(\tilde{x})$ (Gaussian)
0.975-0.980	$0.9714^{+0.0164}_{-0.0170}$
0.980-0.985	$0.9794^{+0.0146}_{-0.0151}$
0.985-0.990	$0.9886^{+0.0140}_{-0.0145}$
0.990-0.995	$0.9793^{+0.0133}_{-0.0139}$
0.995-1.000	$0.9678^{+0.0130}_{-0.0134}$

t (μs)	$P_\mu A(\tilde{x})G(t)$
0.44	$1.0006^{+0.0114}_{-0.0119}$
1.09	$0.9491^{+0.0147}_{-0.0151}$
1.75	$0.9863^{+0.0149}_{-0.0158}$
2.40	$0.9584^{+0.0180}_{-0.0189}$
3.05	$0.9359^{+0.0227}_{-0.0238}$
3.71	$0.9724^{+0.0268}_{-0.0282}$
4.36	$0.9315^{+0.0317}_{-0.0334}$
5.01	$0.9338^{+0.0341}_{-0.0364}$
5.67	$1.0186^{+0.0295}_{-0.0358}$
6.32	$0.8217^{+0.0566}_{-0.0598}$
6.97	$0.9673^{+0.0533}_{-0.0598}$
7.63	$0.9587^{+0.0599}_{-0.0677}$
8.28	$0.9426^{+0.0674}_{-0.0800}$
9.10	$0.9246^{+0.0772}_{-0.0884}$

Table (C.1) cont.

Run Period 3; Target = Al; B_T = 110-G; Events Fitted = 98282

x Range	$P_\mu A(\tilde{x})$ Gaussian	$P_\mu A(\tilde{x})$ Kubo-Tomita
0.88-0.90	$0.9766^{+0.0169}_{-0.0171}$	$0.9837^{+0.0181}_{-0.0180}$
0.90-0.92	$0.9800^{+0.0143}_{-0.0144}$	$0.9864^{+0.0155}_{-0.0153}$
0.92-0.94	$1.0225^{+0.0118}_{-0.0120}$	$1.0295^{+0.0135}_{-0.0131}$
0.94-0.96	$0.9894^{+0.0104}_{-0.0105}$	$0.9963^{+0.0122}_{-0.0117}$
0.96-0.98	$0.9824^{+0.0088}_{-0.0090}$	$0.9894^{+0.0110}_{-0.0103}$
0.98-1.00	$1.0009^{+0.0069}_{-0.0071}$	$1.0080^{+0.0097}_{-0.0087}$
Mean $P_\mu A(\tilde{x})$	$0.9942^{+0.0042}_{-0.0042}$	$1.0014^{+0.0049}_{-0.0049}$
	χ^2_{1220}= 1241.78	χ^2_{1219}= 1239.12

$\cos\theta_e$ Range	$P_\mu A(\tilde{x})$ (Gaussian)
0.975-0.980	$0.9994^{+0.0105}_{-0.0108}$
0.980-0.985	$1.0095^{+0.0097}_{-0.0099}$
0.985-0.990	$0.9918^{+0.0093}_{-0.0096}$
0.990-0.995	$0.9820^{+0.0090}_{-0.0092}$
0.995-1.000	$0.9916^{+0.0086}_{-0.0088}$

t (μs)	$P_\mu A(\tilde{x})G(t)$
0.44	$0.9996^{+0.0072}_{-0.0074}$
1.09	$0.9884^{+0.0085}_{-0.0087}$
1.75	$0.9763^{+0.0100}_{-0.0103}$
2.40	$0.9579^{+0.0120}_{-0.0123}$
3.05	$0.9565^{+0.0140}_{-0.0144}$
3.71	$0.9400^{+0.0169}_{-0.0174}$
4.36	$0.9360^{+0.0193}_{-0.0200}$
5.01	$0.8937^{+0.0234}_{-0.0243}$
5.67	$0.8192^{+0.0298}_{-0.0308}$
6.32	$0.8626^{+0.0326}_{-0.0339}$
6.97	$0.8783^{+0.0402}_{-0.0420}$
7.63	$0.8546^{+0.0437}_{-0.0457}$

Table (C.1) cont.

Run	Target	B_T(G)	$\chi^2_{9,9}$	$P_\mu A(\tilde{x})$	Statistical Error	
194	Ag	70	851.1	1.0172	+0.0213	-0.0235
206	Ag	70	888.4	1.0022	+0.0178	-0.0192
214	Ag	70	910.7	0.9728	+0.0191	-0.0202
228	Ag	70	893.7	1.0013	+0.0170	-0.0178
316	Ag	70	841.3	1.0484	+0.0156	-0.0181
340	Ag	70	924.9	1.0007	+0.0178	-0.0190
352	Ag	70	962.7	1.0158	+0.0153	-0.0165
183	Al	70	846.8	1.0029	+0.0161	-0.0174
199	Al	70	839.8	1.0089	+0.0289	-0.0315
200	Al	70	836.1	0.9813	+0.0232	-0.0250
209	Al	70	872.1	0.9696	+0.0191	-0.0202
234	Al	70	941.9	0.9671	+0.0190	-0.0198
292	Al	70	923.2	1.0078	+0.0192	-0.0205
308	Al	70	867.8	0.9890	+0.0215	-0.0230
317	Al	70	890.5	0.9603	+0.0213	-0.0226
347	Al	70	899.7	0.9866	+0.0178	-0.0192
186	Au	70	896.8	0.9449	+0.0225	-0.0237
210	Au	70	950.9	1.0053	+0.0191	-0.0203
220	Au	70	916.8	1.0093	+0.0149	-0.0162
312	Au	70	976.3	1.0169	+0.0186	-0.0208
324	Au	70	908.4	1.0317	+0.0151	-0.0172
348	Au	70	905.4	1.0065	+0.0173	-0.0186
191	Cu*	70	862.0	1.0079	+0.0247	-0.0269
205	Cu*	70	870.9	0.9972	+0.0180	-0.0194
213	Cu*	70	936.1	0.9922	+0.0184	-0.0196
227	Cu*	70	930.9	1.0268	+0.0131	-0.0146
313	Cu*	70	868.9	1.0038	+0.0180	-0.0196
339	Cu*	70	916.2	0.9898	+0.0196	-0.0207
353	Cu*	70	849.7	1.0023	+0.0176	-0.0185
233	He	70	887.2	0.8509	+0.0228	-0.0233
235	He	70	911.2	0.8924	+0.0215	-0.0222
240	He	70	952.7	0.8838	+0.0237	-0.0245
241	He	70	882.4	0.8575	+0.0244	-0.0251
245	He	70	812.0	0.8609	+0.0410	-0.0427
251	He	70	903.1	0.8467	+0.0255	-0.0262
301	He	70	947.0	0.8645	+0.0253	-0.0261
325	He	70	943.3	0.9561	+0.0229	-0.0240
362	He	70	838.7	0.8728	+0.0350	-0.0363

Table (C.2)...

Run	Target	B_T(G)	χ^2_{1451}	$P_\mu A(\tilde{x})$	Statistical Error	
409	Al	70	1478.1	1.0126	+0.0147	-0.0154
411	Al	70	1542.3	1.0186	+0.0145	-0.0151
419	Al	70	1444.5	1.0138	+0.0180	-0.0191
434	Al	70	1541.5	0.9559	+0.0187	-0.0193
435	Al	70	1487.7	0.9794	+0.0185	-0.0192
442	Al	70	1512.2	0.9723	+0.0185	-0.0192
443	Al	70	1530.0	0.9998	+0.0193	-0.0202
454	Al	70	1514.8	0.9789	+0.0172	-0.0180
468	Al	70	1544.3	0.9801	+0.0198	-0.0207
469	Al	70	1435.4	1.0254	+0.0184	-0.0194
492	Al	70	1515.0	0.9959	+0.0133	-0.0138
503	Al	70	1499.9	0.9914	+0.0149	-0.0154
504	Al	70	1394.3	0.9932	+0.0140	-0.0146
517	Al	70	1512.4	1.0027	+0.0153	-0.0160
518	Al	70	1494.6	0.9953	+0.0182	-0.0189
529	Al	70	1557.4	1.0095	+0.0173	-0.0181
530	Al	70	1535.2	0.9931	+0.0167	-0.0174
541	Al	70	1424.7	1.0091	+0.0167	-0.0174
542	Al	70	1507.2	1.0131	+0.0175	-0.0183
549	Al	70	1489.3	0.9912	+0.0171	-0.0177
550	Al	70	1544.7	0.9856	+0.0171	-0.0181
561	Al	70	1470.5	1.0068	+0.0149	-0.0156
562	Al	70	1444.4	0.9723	+0.0173	-0.0180
579	Al	110	1557.1	1.0074	+0.0149	-0.0159
580	Al	110	1532.1	1.0249	+0.0166	-0.0173
592	Al	110	1412.0	1.0186	+0.0131	-0.0141
593	Al	110	1522.8	0.9752	+0.0161	-0.0167
619	Al	110	1489.9	0.9784	+0.0181	-0.0188
620	Al	110	1373.0	0.9748	+0.0190	-0.0197
716	Al	110	1487.7	0.9887	+0.0172	-0.0178
717	Al	110	1479.2	1.0202	+0.0149	-0.0159
723	Al	110	1474.6	0.9821	+0.0174	-0.0182
724	Al	110	1534.0	0.9948	+0.0165	-0.0173
663	Al*	110	1425.1	1.0222	+0.0150	-0.0163
664	Al*	110	1502.8	0.9605	+0.0185	-0.0191
673	Al*	110	1464.3	1.0014	+0.0160	-0.0170
674	Al*	110	1523.2	0.9804	+0.0168	-0.0175
691	Al*	110	1472.2	1.0020	+0.0164	-0.0172
692	Al*	110	1464.5	1.0148	+0.0160	-0.0170
699	Al*	110	1572.1	0.9673	+0.0183	-0.0189
700	Al*	110	1440.6	0.9977	+0.0174	-0.0183
707	Al*	110	1518.7	1.0043	+0.0159	-0.0167
708	Al*	110	1549.9	0.9844	+0.0160	-0.0167

Table (C.2) cont.

Run	Target	B_T(G)	$\chi^2_{1\,4\,5\,1}$	$P_\mu A(\tilde{x})$	Statistical Error	
418	Au	70	1390.3	0.9686	+0.0201	-0.0210
430	Au	70	1409.2	0.9790	+0.0156	-0.0165
431	Au	70	1445.2	1.0137	+0.0150	-0.0162
446	Au	70	1443.8	1.0001	+0.0162	-0.0171
447	Au	70	1510.7	1.0090	+0.0132	-0.0143
472	Au	70	1425.3	1.0137	+0.0175	-0.0188
473	Au	70	1421.5	1.0138	+0.0172	-0.0189
495	Au	70	1576.2	1.0020	+0.0143	-0.0150
507	Au	70	1399.5	0.9933	+0.0172	-0.0182
508	Au	70	1474.7	0.9937	+0.0150	-0.0162
521	Au	70	1401.2	1.0115	+0.0139	-0.0147
522	Au	70	1454.3	0.9890	+0.0148	-0.0152
533	Au	70	1414.5	1.0116	+0.0153	-0.0165
534	Au	70	1412.4	0.9682	+0.0183	-0.0190
545	Au	70	1495.5	0.9877	+0.0160	-0.0168
546	Au	70	1529.2	0.9927	+0.0153	-0.0163
553	Au	70	1412.5	1.0017	+0.0165	-0.0174
554	Au	70	1461.5	0.9759	+0.0176	-0.0184
565	Au	70	1538.2	0.9798	+0.0146	-0.0152
566	Au	70	1410.1	0.9999	+0.0170	-0.0181
567	Au	70	1273.9	1.0264	+0.0264	-0.0289
583	Au	110	1535.3	1.0254	+0.0125	-0.0131
584	Au	110	1485.9	0.9834	+0.0147	-0.0152
596	Au	110	1512.4	0.9910	+0.0146	-0.0153
597	Au	110	1448.6	0.9742	+0.0146	-0.0152
414	Cu	70	1356.3	0.9940	+0.0219	-0.0231
415	Cu	70	1515.9	0.9838	+0.0172	-0.0180
426	Cu	70	1457.1	0.9837	+0.0169	-0.0176
427	Cu	70	1456.5	0.9765	+0.0160	-0.0167
440	Cu	70	1400.1	0.9871	+0.0163	-0.0171
441	Cu	70	1526.2	0.9630	+0.0180	-0.0187
450	Cu	70	1445.7	0.9691	+0.0187	-0.0194
451	Cu	70	1458.4	0.9786	+0.0181	-0.0189
464	Cu	70	1448.7	0.9796	+0.0166	-0.0175
465	Cu	70	1500.4	0.9940	+0.0174	-0.0185
487	Cu	70	1531.3	1.0075	+0.0117	-0.0123
488	Cu	70	1462.8	0.9740	+0.0174	-0.0182
489	Cu	70	1497.0	0.9933	+0.0138	-0.0143
499	Cu	70	1409.1	0.9658	+0.0234	-0.0247
500	Cu	70	1531.3	0.9954	+0.0154	-0.0162
513	Cu	70	1421.6	0.9909	+0.0146	-0.0152
514	Cu	70	1430.2	0.9985	+0.0143	-0.0150

Table (C.2) cont.

Run	Target	B_T(G)	χ^2_{1451}	$P_\mu A(\tilde{x})$	Statistical Error	
525	Cu	70	1437.6	0.9686	+0.0156	-0.0164
526	Cu	70	1458.8	0.9755	+0.0185	-0.0192
537	Cu	70	1412.3	0.9984	+0.0162	-0.0171
538	Cu	70	1511.5	0.9830	+0.0169	-0.0178
557	Cu	70	1473.8	0.9769	+0.0173	-0.0181
558	Cu	70	1474.8	0.9945	+0.0169	-0.0176
575	Cu	110	1520.0	0.9920	+0.0118	-0.0122
576	Cu	110	1612.0	0.9629	+0.0165	-0.0171
588	Cu	110	1442.1	0.9903	+0.0140	-0.0147
589	Cu	110	1531.7	0.9711	+0.0144	-0.0149
712	Cu	110	1446.6	0.9705	+0.0162	-0.0169
713	Cu	110	1503.2	0.9587	+0.0166	-0.0172
600	Cu*	110	1481.2	0.9683	+0.0158	-0.0164
601	Cu*	110	1473.0	0.9747	+0.0172	-0.0180
669	Cu*	110	1533.0	0.9993	+0.0159	-0.0167
695	Cu*	110	1507.4	0.9529	+0.0183	-0.0190
696	Cu*	110	1497.5	0.9869	+0.0182	-0.0189
703	Cu*	110	1433.1	0.9744	+0.0156	-0.0163
704	Cu*	110	1520.9	0.9858	+0.0163	-0.0170

Run	Target	B_T(G)	χ^2_{1229}	$P_\mu A(\tilde{x})$	Statistical Error	
883	Al	110	1305.1	1.0018	+0.0175	-0.0183
884	Al	110	1271.9	0.9703	+0.0153	-0.0158
890	Al	110	1353.9	1.0101	+0.0144	-0.0151
896	Al	110	1400.9	1.0033	+0.0132	-0.0139
903	Al	110	1325.9	1.0038	+0.0150	-0.0156
909	Al	110	1303.9	0.9900	+0.0140	-0.0145
914	Al	110	1285.5	1.0112	+0.0149	-0.0155
921	Al	110	1197.7	0.9859	+0.0163	-0.0169
928	Al	110	1357.0	1.0074	+0.0128	-0.0133
934	Al	110	1359.3	0.9908	+0.0126	-0.0131
940	Al	110	1346.3	0.9957	+0.0135	-0.0140
947	Al	110	1363.6	0.9620	+0.0149	-0.0153

Table (C.2) cont.

References

1. S.L. Glashow, Nucl. Phys. 22, 579 (1961).
2. S. Weinberg, Phys. Rev. Lett. 19, 1264 (1967).
3. A. Salam, Proc. 8th Nobel Symposium, Aspenasgarden (Almqvist and Wiskell, Stockholm, 1968).
4. E.M. Lipmanov, Yad. Fiz. 6, 541 (1967) [Sov. J. Nucl. Phys. 6, 395 (1968)].
5. J.C. Pati and A. Salam, Phys. Rev. Lett. 31, 661 (1973) and Phys. Rev. D10, 275 (1974).
6. R.N. Mohapatra and J.C. Pati, Phys. Rev. D11, 566, 2588 (1975).
7. G. Senjanovic and R.N. Mohapatra, Phys. Rev. D12, 1502 (1975).
8. A.E. Pifer et al., Nucl. Instr. Meth. 135, 39 (1976).
9. J. Carr et al., Phys. Rev. Lett. 51, 627 (1983).
10. G. Arnison et al., Phys. Lett. 122B, 103 (1983) and 126B, 398 (1983).
11. M. Banner et al., Phys. Lett. 122B, 476 (1983).
12. W.J. Marciano and A. Sirlin, Phys. Rev. D29, 945 (1984).
13. G. Senjanovic, Nucl. Phys. B153, 334 (1979).
14. M. Gell-Mann, P. Ramond and R. Slansky, unpublished.
15. R.N. Mohapatra and G. Senjanovic, Phys. Rev. Lett. 44, 912 (1980) and Phys. Rev. D23, 165 (1981).
16. H. Abramowicz et al., Z. Phys. C12, 225 (1982).
17. Primary input to the world average is V.V. Akhmanov et al., Yad. Fiz. 6, 316 (1967) [Sov. J. Nucl. Phys. 6, 230 (1968)].
18. Primary input to the world average is J. Peoples, Nevis Cyclotron Report No. 147 (1966).

19. J. Van Klinken, Nucl. Phys. 75, 145 (1966).

20. J. Van Klinken et al., Phys. Rev. Lett. 50, 94 (1983).

21. D. Schreiber and F.T. Calaprice, private communication; D. Schreiber, Ph.D. thesis, Princeton University, 1983 (unpublished); F.T. Calaprice et al., Phys. Rev. Lett. 35, 1566 (1975).

22. T. Vitale et al. (unpublished) quoted by B.R. Holstein and S.B. Treiman, Phys. Rev. D16, 2369 (1977).

23. L. Wolfenstein, Phys. Rev. D29, 2130 (1984).

24. J. Donahue and B. Holstein, Phys. Lett 113B, 382 (1982). See also I.I. Bigi and J.M. Frere, Phys. Lett. 110B, 255 (1982).

25. G. Beall et al., Phys. Rev. Lett. 48, 848 (1982).

26. F.J. Gilman and M.H. Reno, Phys. Lett. 127B, 426 (1983).

27. P. DeForcrand, Ph.D. thesis, Univ. of Calif., Berkeley (1982), Lawrence Berkeley Laboratory Report No. LBL-14692.

28. T.D. Lee and C.N. Yang, Phys. Rev. 108, 1611 (1957).

29. F. Scheck, Phys. Lett. C44, 187 (1978).

30. A.M. Sachs and A. Sirlin, in Muon Physics, Vol. II, V. Hughes and C.S. Wu, eds. (Academic Press, N.Y., 1975), p.50.

31. C.G. Wohl et al. (Particle Data Group), Rev. Mod. Phys. 56, S1 (1984). Primary input to ρ is Ref. 18; primary input to η is F. Corriveau et al., Phys. Lett. 129B, 260 (1983) and S.E. Derenzo, Phys.Rev. 181, 1854 (1969); primary input to ξP_μ is Ref. 17; primary input to $\xi P_\mu \delta/\rho$ is Ref. 9; primary input to δ is D. Fryberger, Phys. Rev. 166, 1379 (1968).

32. M.A.B. Beg et al., Phys. Rev. Lett. 38, 1252 (1977).

33. W.E. Fischer and F. Scheck, Nucl. Phys. B83, 25 (1974).

34. V. Florescu and O. Kamei, Nuovo Cimento 61A, 967 (1968).

35. M.A.B. Beg and A. Sirlin, Ann. Rev. Nucl. Sci. 24, 579 (1974).

36. K. Mursula and F. Scheck, Nucl. Phys. B253, 189 (1985).

37. J.H. Brewer et al., in Muon Physics, Vol. III, V. Hughes and C.S. Wu eds. (Academic Press, N.Y., 1975), p.4.

38. G.W. Ford and C.J. Mullin, Phys. Rev. 108, 477 (1957).

39. V. Hughes, Phys. Rev. 108, 1106 (1957).

40. Proceedings of recent μSR conferences are contained in Hyperfine Interactions 6 (1979) and 17-19 (1984).

41. D. Richter, in Neutron Scattering and Muon Spin Rotation, Springer Tracts in Modern Physics 101 (Springer-Verlag 1983) p.85.

42. R. Kubo and K. Tomita, J. Phys. Soc. Jpn 9, 888 (1954).

43. J.H. van Vleck, Phys. Rev. 74, 1168 (1948).

44. K.W. Kehr et al., Z. Phys. B32, 49 (1978).

45. A.P. Mills, Proc. 6th Int. Conf. on Positron Annihilation, P.G. Coleman, S.C. Sharma, and L.M. Diana eds. (North-Holland, Amsterdam 1982) p.121.

46. C.J. Oram et al., Nucl. Instr. Meth. 179, 95 (1981).

47. R. Sagane et al., Phys. Rev. 95, 863 (1954).

48. K. Halbach, private communication.

49. Y.S. Tsai, SLAC-PUB-848 (1971).

50. B.P. Nigam et al., Phys. Rev. 115, 491 (1959).

51. J.B. Marion and B.A. Zimmerman, Nucl. Instr. Meth. 51, 93 (1967).

52. A.P. Rekalo, Ukr. Fiz. Zh. 16(12), 1937 (1971) and Yad. Fiz. 13(6), 1288 (1971) [Sov. J. Nucl. Phys. 13(6) 741 (1971)].

53. B. Balke et al., Lawrence Berkeley Laboratory Report No. LBL-18320.

54. M. Abolins et al., Proc. 1982 DPF Summer Study Elem. Part. Phys. and Future Facilities p.274 (Snowmass, 1982).

55. E.J. Eichten et al., Phys. Rev. Lett. 50, 811 (1983).

56. M.E. Peskin, private communication.

57. K.D. Lane and E. Barany, private communication.